Theoretical Notes
Note 301

TN 301

AMRC-R-159
Copy _____

ANALYTIC APPROXIMATIONS OF X-RAY DEPOSITION REGION COUPLING TO MISSILES IN FLIGHT

J. Gilbert
E. Pettus
J. Dancz
W. Hobbs

October 1978

Prepared For: Air Force Weapons Laboratory
Kirtland Air Force Base
New Mexico 87117

Under Contract: F29601-77-C-0020
Subtask 01-06

This project has been partially supported by the Defense Nuclear Agency (DNA) under:

DNA Subtask R99QAXEB088
EMP Interaction and Coupling
DNA Work Unit 84
Survey of Close-In Coupling Techniques
and Associated Accuracies

Prepared by: MISSION RESEARCH CORPORATION
1400 San Mateo Boulevard, S. E.
Suite A
Albuquerque, New Mexico 87108

SECURITY CLASSIFICATION OF THIS PAGE (When Data Entered)

REPORT DOCUMENTATION PAGE

READ INSTRUCTIONS BEFORE COMPLETING FORM

1. REPORT NUMBER	2. GOVT ACCESSION NO. / 3. RECIPIENT'S CATALOG NUMBER
4. TITLE (and Subtitle): ANALYTIC APPROXIMATIONS OF X-RAY DEPOSITION REGION COUPLING TO MISSILES IN FLIGHT	5. TYPE OF REPORT & PERIOD COVERED: Final Report
	6. PERFORMING ORG. REPORT NUMBER: AMRC-R-159
7. AUTHOR(s): J. Gilbert, J. Dancz, E. Pettus, W. Hobbs	8. CONTRACT OR GRANT NUMBER(s): F29601-77-C-0020
9. PERFORMING ORGANIZATION NAME AND ADDRESS: MISSION RESEARCH CORPORATION, 1400 San Mateo Blvd., S. E. Suite A, Albuquerque, New Mexico 87108	10. PROGRAM ELEMENT, PROJECT, TASK AREA & WORK UNIT NUMBERS
11. CONTROLLING OFFICE NAME AND ADDRESS: Air Force Weapons Laboratory, Kirtland Air Force Base, New Mexico 87117	12. REPORT DATE: October 1978 13. NUMBER OF PAGES: 59
14. MONITORING AGENCY NAME & ADDRESS (if different from Controlling Office)	15. SECURITY CLASS. (of this report): Unclassified 15a. DECLASSIFICATION DOWNGRADING SCHEDULE

16. DISTRIBUTION STATEMENT (of this Report)

17. DISTRIBUTION STATEMENT (of the abstract entered in Block 20, if different from Report)

18. SUPPLEMENTARY NOTES

19. KEY WORDS (Continue on reverse side if necessary and identify by block number)

EMP
SGEMP
Close-in-coupling
X-ray Deposition Region
Missiles in Flight

20. ABSTRACT (Continue on reverse side if necessary and identify by block number)

In this report we present a number of calculations relevant to the generation of electromagnetic fields when weapon X-rays impinge on missiles in flight above about 60 km. In this altitude regime the motion of secondary electrons is not dominated by collisions with neutral atoms and electrostatic and electromagnetic oscillations are seen. We calculate the response of a flat conducting surface in two time regimes; in the first time regime the fields are driven by photoelectrons emitted from the surface. In the

DD FORM 1 JAN 73 1473 EDITION OF 1 NOV 65 IS OBSOLETE

SECURITY CLASSIFICATION OF THIS PAGE (When Data Entered)

second time regime the fields are driven by photoelectrons produced in the air. We also calculate the response of a simple model of a monopole antenna exposed to X-rays.

CONTENTS

ILLUSTRATIONS

SECTION I

INTRODUCTION

In this report we derive approximate analytic expressions for electromagnetic fields near conducting surfaces caused by the interaction of high fluence (multicalorie/cm^2) X-rays with the surface materials and surrounding atmosphere. The atmospheric pressures considered are less than 0.1 torr, as the goal of these calculations is the analysis of the survivability of a missile in flight at altitudes greater than about 60 km. The fluences and X-ray energies considered are such that, in vacuum, the photoelectrons emitted from surface materials would space charge limit in distances much smaller than typical object radii of curvature in a time scale much shorter than the duration of the X-ray pulse.

The use of numerical techniques to analyze the electromagnetic fields near missile surfaces in this regime has been in progress for about a year before the preparation of this report, and two of the analytic calculations presented here were derived in an earlier report*. There are a number of reasons for proceeding with both numerical and analytical techniques. The numerical techniques are capable of including effects such as velocity-dependent momentum transfer cross sections that are not tractable analytically, are more accurate when there are opposing physical effects with comparable magnitudes and time and distance scales, and are capable of working with much more complex geometries. The analytic techniques are more capable of combining physical effects with greatly disparate time and distance scales and serve to guide one in the construction of numerical techniques; they directly tell one what are the relevant physical effects and time and distance scales. In addition, they permit one to check the accuracy of his numerical code by calculating an exactly solvable case.

There are basically two physical effects which create electromagnetic fields in the vicinity of a missile in flight. The first of these is

*Gilbert, J. L., W. E. Hobbs and H. J. Price (to be published).

caused by photoemission of electrons from the missile surface, and is known for historical reasons as system-generated electromagnetic pulse (SGEMP). The motion of these photoelectrons causes EM fields and skin currents which can drive currents on conductors connected to electronic circuitry and thus damage them. These EM fields also modify the motion of these photoelectrons and so require a simultaneous solution of the electron motion and electromagnetic fields. In the case with which we are interested here, the electric fields become so large that the emitted electrons are driven back into the surface on an extremely short time scale after travelling only a few millimeters from the missile surface. This allows us to treat the conducting missile surface as locally flat and compute the normal electric field near the surface as the solution of a planar electrostatics problem. The low velocity of the electrons relative to the speed of light allows us to also ignore the effects of the magnetic field upon the electron trajectories. (The time required for an electron to complete a Larmor orbit in the earth's magnetic field is about 10^{-6} sec. All the effects which we consider in this report occur on a time scale less than 10^{-7} sec.) Within these approximations, and using the results of previous studies of vacuum SGEMP, we can solve for the magnetic fields which result from this effect and we find that they dominate at early times, peaking much before the peak of the X-ray pulse. The reason for this is that once the surface photoelectrons space charge limit, the returning current nearly cancels the emitted current so that there is little $\nabla \times J$ which drives the magnetic field.

The second physical effect is the ejection of photoelectrons from the atmosphere. These electrons are ejected with a slight correlation between the directions of the incident photon and the ejected electron, giving rise to a net current in the direction of the X-ray source. (There are also strong currents arising at the interfaces between exposed and shadowed regions which we will examine here.) This effect is analogous to currents on conductors caused by gamma rays at ground level and referred to as close-in-coupling (CIC); in our case it will dominate the late time magnetic

fields. The surface magnetic fields resulting from this effect have a waveform similar to the time integral of the X-ray pulse, rather than one similar to the X-ray pulse itself. The reason for this is that the drag forces on the photoelectrons, caused by collisions between the photoelectrons and the neutral atoms in the ambient atmosphere, are small so that the photocurrent continues to rise through the entire X-ray pulse. (The time required for the drag forces to appreciably slow a 10 keV primary photoelectron is on the order of 200 nanoseconds.) This is dependent on the air photoelectrons not space charge limiting in their own electric fields; space charge limiting does not occur for two reasons -- the ionization existing before the X-ray pulse arrives is sufficient to prevent space charge limiting when this ionization electron density is substantially greater than the photoelectron density, and the presence of the conducting missile skin reduces electric fields parallel to the surface near the surface.

At higher pressure regimes than the one which we consider, the collisional drag on secondary electrons is sufficiently large that their velocity is determined by the balance of the accelerations due to the electric field and the collisional drag. In our regime (pressures below 0.1 torr), the electron momentum becomes more important than the drag and at early times a cold collisionless plasma is a good model. For later times at the lower altitudes in this regime the collisional drag on secondaries becomes important. It is never important here for photo primaries due to their larger energies.

The remainder of this report is organized in four sections on analytic approximations to the environment (ionization and photo currents), early time effects, late time effects and an example of coupling to local geometries.

In this report we work in cgs Gaussian units, but give typical results in MKS units. Some useful conversion formulae are:

Electric field	$E\left(\frac{\text{volts}}{\text{meter}}\right) = 3\times10^{4}\ E(\text{esu})$
Magnetic Field	$B(\text{teslas}) = 10^{-4}\ B(\text{gauss})$
Current	$I(\text{amps}) = \frac{1}{3}\times10^{-9}\ I(\text{esu/sec})$
Conductivity	$\sigma\left(\frac{\text{siemens}}{\text{m}}\right) = \frac{1}{9}\times10^{-9}\ \sigma(\text{sec}^{-1})$

SECTION II

ENVIRONMENTS

In this section we discuss the approximate calculation of the quantities which determine the electromagnetic fields. These quantities are:

1) Energy deposition of X-rays in the air.
2) Surface electron emission.
3) Air photocurrents.

1. ENERGY DEPOSITION

The total energy deposition in the air is important as it determines the ionization present about the missile from previous X-ray pulses; there will, in addition, be ionization created by the photoelectrons ejected from the air and surface by the X-ray pulse which is arriving at the times of interest. The pre-existing ionization is the more important in determining the modification of the early time SGEMP response; which of the two sources of ionization is more important in determining the late time behavior of the surface magnetic fields is dependent on the altitude and the relative temperatures of the X-rays of interest. We will first discuss the ionization created by previous X-ray pulses. This ionization is relatively constant over times of interest; we will defer the discussion of the ionization created by the arriving pulse until the last part of this section.

The mechanism for producing ionization is the ejection of photoelectrons by the incident X-rays followed by the production of free secondary electrons as the photoelectron is slowed down. As the photoelectron is almost always ejected from the K-shell, it is ejected with the photon energy minus the binding energy (about 600 eV) which is small compared to the photon energy. The photoelectron then loses energy, producing about one secondary for every 86 eV of energy loss (ref. 1). Each of these secondaries in additional collisions produces on the average about two additional secondaries for a total of one secondary for each 34 eV of energy deposited.

1. Longmire, C. L. and H. J. Longley, Improvements in the Treatment of Compton Current and Air Conductivity in EMP Problems, DNA 3192T, Defense Nuclear Agency, September 1973.

We have developed a simple method to evaluate the energy absorbed. Let I(E)dE be the X-ray energy (keV) in the interval E to E + dE produced by the bomb. In travelling out to a distance R from the detonation, the X-rays will be attenuated by both $1/r^2$ and absorption in the atmosphere. At a distance R from the burst, the X-ray packet will have a fluence of

$$F(E)dE = \frac{\exp[-\sigma(E)L]\ I(E)dE}{4\pi R^2} \tag{1}$$

where $L(gm/cm^2)$ is the integrated air mass between the detonation point and the point R,

$$L = \int_0^R \rho(r)dr\ , \tag{2}$$

and $\sigma(cm^2/gm)$ is the mass attenuation coefficient for the X-rays of energy E. The differential energy absorbed $dW(keV/cm^3)$ is therefore,

$$dW = \rho\sigma F(E)dE \tag{3}$$

where ρ is the local air density, and the total energy absorbed is simply the integral of this.

In fact, this integral may be approximately evaluated in a straightforward manner. The energy spectrum is essentially a blackbody and the high energy part of the spectrum may be approximated as a cubic times an exponential. A reasonable approximation of the spectrum is given by

$$I(E) = \frac{I_o}{6T^4} E^3 \exp(-E/T) \tag{4}$$

where I_o is the total energy in the spectrum and T is the blackbody temperature in kilovolts. At high photon energies the atmospheric photoelectric absorption coefficient is well approximated by

$$\sigma = \alpha/E^3 \tag{5}$$

where $\alpha = 3 \times 10^3$ keV^3 cm^2/gm. This is a good approximation from above the oxygen K-edge at 0.56 keV up to above 40 keV where Compton scattering becomes dominant, so it covers the energy of our X-rays. Since the third powers of E cancel, the integral for the total energy absorbed becomes

$$W = \frac{\rho\alpha I_o}{24\pi R^2 T^4} \int_0^\infty \exp[-(\frac{E}{T} + \frac{\alpha L}{E^3})]dE \tag{6}$$

The exponent in the integral has a maximum value at

$$E_m = (3\alpha LT)^{1/4} \tag{7}$$

If this is somewhat higher than the radiation temperature, then the integral can be approximately evaluated using the saddle point method (ref. 2),

$$W \simeq \frac{\rho\alpha I_o}{24\pi R^2 T^4} \sqrt{\frac{\pi E_m T}{2}} \exp(-4E_m/3T) \tag{8}$$

In preionization cases of interest W can range up to about 10^{-8} cal/cm^3 resulting in electron densities up to 4×10^9 electons/cm^3.

2. SURFACE PHOTOEMISSION

This method can also be used to estimate the surface photoemission. As discussed previously, the photoelectric cross section behaves as $1/E^3$. The range of electrons in materials in this energy range behaves as E^2 so the electron yield from a surface for monoenergetic photons behaves as $1/E$ electrons/photon or $1/E^2$ electrons/keV. From the tables of Dellin and McCallum (ref. 3), these yields for carbon and aluminum are

$$Y_C = 0.026 \frac{1}{E_x^2} \text{ electrons/keV} \tag{9}$$

$$Y_{Al} = 0.340 \frac{1}{E_x^2} \text{ electrons/keV} \tag{10}$$

2. Morse, P. M. and H. Feshbach, Methods of Theoretical Physics, McGraw-Hill, 1953.
3. Dellin, T. A. and C. J. MacCallum, Handbook of Photocompton Current Data, SCL-PR-720056, Sandia Laboratories, 1972.

where E_x is in keV. If the device X-ray output is $I_1(t)$ keV/sec, the current density emitted from the surface is

$$J(t) = \frac{eYI_1(t)}{24\pi R^2 T^4} \int_0^\infty E \exp\left[-\left(\frac{E}{T} + \frac{\alpha L}{E^3}\right)\right] dE \qquad (11)$$

$$\sim \frac{eYI_1(t)E_m}{24\pi R^2 T^4} \sqrt{\frac{\pi E_m T}{2}}\ e^{-4E_m/3T}$$

for $E_m \gtrsim T$. The actual velocity distribution of the emitted photoelectrons is more complicated -- there are a couple of limiting cases which are reasonably simple. The first of these is where there is little attenuation, $E_m \ll T$. This is the usual case in satellite SGEMP and the resulting photoelectron distribution is exponential in energy with a characteristic energy near the X-ray temperature and has a $\cos\theta$ angular distribution where θ is the angle between the surface normal and the ejected photoelectron. The other case is where $E_m \gg T$ so that the distribution of photons incident on the surface is sharply peaked about E_m. In this case the emitted electron energy distribution is nearly triangular (ref. 4) as shown below, with a $\cos\theta$ angular distribution. In cases of interest, the surface photoemission can produce emitted currents up to about 1000 amperes/cm^2.

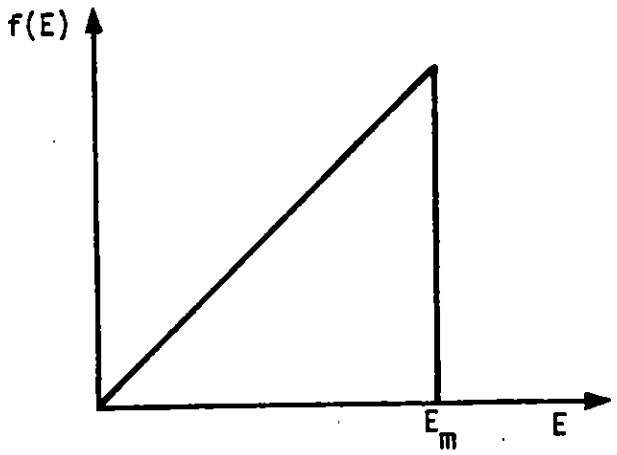

Figure 1. Electron Energy Distribution for Monoenergetic Photons

4. Schaefer, R., "A Simple Model for Soft X-ray Photoemission," Jo. App. Phys., 44, 1973.

3. AIR PHOTOCURRENTS

Next we calculate the sources of primary photocurrents and secondary ionization. We first examine the angular distribution of photoemission. From reference 5 the angular distribution is proportional to

$$\phi = \frac{1 - \mu^2}{(1 - \beta\mu)^4} \tag{12}$$

where μ is the cosine of the angle between the incident photon and the ejected electron, and $\beta = v_e/c$, where v_e is the velocity of the emitted electron. For small β we can expand

$$\phi \sim (1 - \mu^2)(1 + 4\beta\mu) \tag{13}$$

and

$$\bar{\mu}(\beta) = \frac{\int_{-1}^{1} \mu\phi(\beta,\mu)d\mu}{\int_{-1}^{1} \phi(\beta,\mu)d\mu} \sim \frac{4}{5}\beta \tag{14}$$

If we are far from material discontinuities we can use the fact that our electrons are slowly moving with respect to c and write

$$\frac{\partial J_p}{\partial t} = - e \int_0^\infty dE\ \mu(E)\ v_e(E)\ \frac{\partial \rho_p(E)}{\partial t} \tag{15}$$

where $\frac{\partial \rho_p(E)}{\partial t}$ is the rate at which photoprimaries of energy E are being created in electrons/cm^3-sec. From our discussion of energy absorption we easily have $\partial\rho_p/\partial t$,

$$\frac{\partial \rho_p(E)}{\partial t} = \frac{\rho\alpha I_1(t)}{24\pi R^2 T^4}\ \frac{1}{E}\ e^{-(E/T + \alpha L/E^3)} \tag{16}$$

and for nonrelativistic velocities

$$\bar{\mu}(E)\ v_e(E) = \frac{4v_e^2}{5c} = \frac{8E}{5mc} \tag{17}$$

5. Heitler, W., The Quantum Theory of Radiation, Oxford University Press, London, 1954.

The energy integral can again be evaluated by the saddle point method for $E_m \gtrsim T$, yielding

$$\frac{\partial J_p}{\partial t} \sim - \frac{e\rho\alpha\, I_1(t)}{15\pi mcR^2T^4} \sqrt{\frac{\pi E_m T}{2}}\; e^{-4E_m/3T} \tag{18}$$

A typical value of the peak of J_p is 1000 amps/m^2. We find the rate of the production of secondary ionization from the energy loss of photoprimaries. The extreme range of electrons in air is fit between 3 and 30 keV by (ref. 6)

$$R \sim \frac{C}{\rho} E^2 \tag{19}$$

where

$$C \sim 2.5 \times 10^{-6} \frac{gm}{cm^2 - keV^2}$$

so that

$$\frac{dE}{dt} = \frac{\rho}{2CE} \frac{dR}{dt} = \frac{\rho}{C\sqrt{2mE}} \tag{20}$$

for each electron. If W_I is the energy loss of a photoprimary required to produce a secondary electron, the production rate of the secondaries is

$$\frac{\partial \rho_s}{\partial t} = \frac{\rho^2\alpha \int_0^t I_1(t')dt'}{24\pi C W_I R^2 T^4 \sqrt{2m}} \int_0^\infty \frac{dE}{E^{3/2}}\; e^{-(E/T + \alpha L/E^3)} \tag{21}$$

which is approximately, again using the saddle point method,

$$\frac{\partial \rho_s}{\partial t} = \frac{\rho^2\alpha \int_0^t I_1(t')dt'}{48\pi C W_I R^2 T^4 E_m} \sqrt{\frac{\pi T}{m}}\; e^{-4E_m/3T} \tag{22}$$

during times of interest, a typical value of ρ_s is about 10^{10} electrons/cm^3.

6. Evans, R. D., The Atomic Nucleus, McGraw-Hill, 1955.

The final calculation is of the current caused by photoelectrons which free stream from an illuminated region into a nonilluminated region. This is important as it describes approximately the sources existing in shadowed regions as well as the alteration of the current in unshadowed regions resulting from presence of nearby shadowed regions. In this calculation we assume that the photoprimaries are freely streaming from their point of origin. The drag forces on the primaries are small and if the secondary number density is much greater than the primary number density, the effects of the electric field on the motion of the primary electrons are small. We use the geometry shown in figure 2.

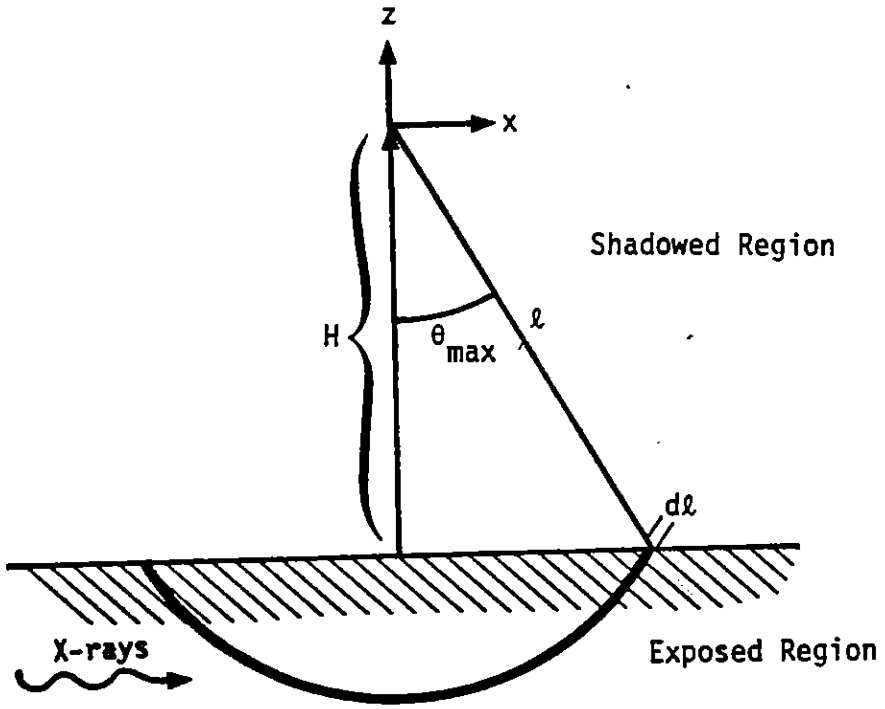

Figure 2. Geometry Used for Transverse Current Calculation

Defining

$$f(\vec{x},v,\vec{\Omega},t)\, dv d\vec{\Omega} = \text{density of primary photoelectrons moving between v and dv within } d\vec{\Omega} \text{ of direction } \vec{\Omega} \text{ (electrons-sec}^3/\text{cm}^6) \quad (23)$$

$$S_o(\vec{x},v,\vec{\Omega},t)\ dvd\vec{\Omega} = \text{source rate of photoprimaries (electrons-sec}^2/\text{cm}^6) \tag{24}$$

The free streaming solution is

$$f(\vec{x},v,\vec{\Omega},t) = \frac{1}{v}\int_0^\infty d\ell\ S_o(\vec{x} - \ell\vec{\Omega},v,\vec{\Omega},t - \ell/v) \tag{25}$$

For our problem, as the electrons are nonrelativistic, we ignore the retardation in time and set

$$S_o = \xi(v)\eta(\vec{\Omega})h(t) \tag{26}$$

where ξ and η are normalized so

$$\int_0^\infty v^2 dv\ \xi(v) = 1 \tag{27}$$

$$\int d\vec{\Omega}\ \eta(\vec{\Omega}) = 1 \tag{28}$$

For low velocity ($\beta<<1$) electrons, we use a $\sin^2\theta_x$ distribution

$$\eta(\Omega) = \frac{3}{8\pi}(1 - \mu^2) \tag{29}$$

where $\mu = \cos\theta_x$, and θ_x is the angle between the incident X-ray and the emitted electron. In our frame where θ is the angle with respect to the z axis

$$\eta(\Omega) = \frac{3}{8\pi}(1 - \sin^2\theta\cos^2\phi) \tag{30}$$

where ϕ is the azimuthal angle in the x-y plane. We calculate the net current

$$J_z(\vec{x},t) = -e\int v_z\, f\, d^3v \tag{31}$$

$$= -e\int_0^\infty v^2 dv \int_H^\infty d\ell\ \xi(v)h(t - \ell/v)\int_{H/\ell}^1 d\mu \int_0^{2\pi} d\phi\ \frac{3\mu}{8\pi}\left[1-(1-\mu^2)\cos^2\phi\right]$$

where $\mu_{min} = H/\ell$ from the figure, and e is the electronic charge.

The angular integrals are readily evaluated

$$\frac{3}{8\pi}\int_{H/\ell}^1 d\mu\ \mu\int_0^{2\pi} d\phi\left[1-(1-\mu^2)\cos^2\phi\right] = \frac{3}{8}\left\{\frac{3}{4} - \frac{H^2}{2\ell^2} - \frac{H^4}{4\ell^4}\right\} \tag{32}$$

Replacing ℓ by $\tau = \ell/v$

$$J = -\frac{3e}{8}\int_0^\infty v^2 dv \int_{H/v}^\infty d\tau\ v\xi(v)h(t - \tau)\left\{\frac{3}{4} - \frac{H^2}{2v^2\tau^2} - \frac{H^4}{4v^4\tau^4}\right\} \tag{33}$$

We can interchange the limits of integration (see figure 3) and we obtain

$$J = -\frac{3e}{8}\int_0^\infty d\tau\ h(t-\tau)\ I(\tau) \tag{34}$$

where

$$I(\tau) = \frac{3}{4}\int_{H/\tau}^\infty dv\ v^3\ \xi(v)$$

$$-\frac{H^2}{2\tau^2}\int_{H/\tau}^\infty dv\ v\ \xi(v) \tag{35}$$

$$-\frac{H^4}{4\tau^4}\int_{H/\tau}^\infty dv\ \xi(v)/v$$

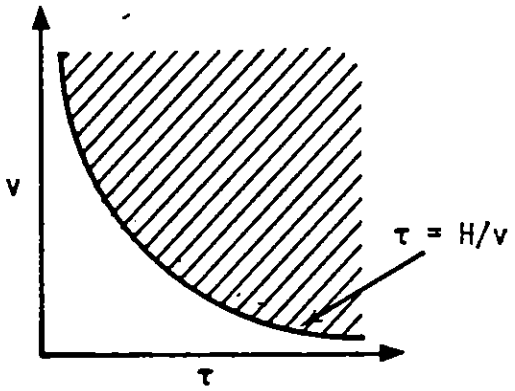

Figure 3. Region of Integration in v-τ Plane

These integrals become simple in a couple of limiting distributions -- the first of these is when there is little air intervening between the burst and the missile. In that case the X-ray flux is an unattenuated black body spectrum and, as the photoelectric cross section behaves as $1/E^3$, the electron spectrum is approximately

$$\xi(v) = \frac{m}{T} \frac{1}{v} e^{-mv^2/2T} \tag{36}$$

The integrals can be evaluated in terms of the error function $\phi(x)$ defined by

$$\phi(x) = \frac{2}{\sqrt{\pi}} \int_0^x e^{-u^2} du \tag{37}$$

The second integral is in this form already and the first and third can be converted into it by integration by parts. The resulting function is

$$\begin{aligned} I(\tau) = {} & \frac{3H}{4\tau} e^{-mH^2/2T\tau^2} + \frac{3}{8} \sqrt{\frac{2\pi T}{m}} \left\{1 - \phi\left(\frac{H}{\tau} \sqrt{\frac{m}{2T}}\right)\right\} \\ & - \frac{H^2}{4\tau^2} \sqrt{\frac{2\pi m}{T}} \left\{1 - \phi\left(\frac{H}{\tau} \sqrt{\frac{m}{2T}}\right)\right\} \\ & - \frac{H^3}{4\tau^3} \frac{m}{T} e^{-mH^2/2T\tau^2} + \frac{H^4}{8\tau^4} \frac{m}{T} \sqrt{\frac{2\pi m}{T}} \left\{1 - \phi\left(\frac{H}{\tau} \sqrt{\frac{m}{2T}}\right)\right\} \end{aligned} \tag{38}$$

where the three lines of the expression here correspond to the three integrals. The other limiting case corresponds to a photon flux that has been greatly attenuated by passage through the air; if $E_m >> T$ the electron velocity is strongly peaked about

$$v_m = \sqrt{\frac{2E_m}{m}} \tag{39}$$

As the time integral will smooth out the behavior of currents, we can treat the velocity distribution as a δ function

$$\xi(v) = \frac{1}{v_m^2}\,\delta(v - v_m) \tag{40}$$

and obtain

$$I(\tau) = \left(\frac{3v_m}{4} - \frac{H^2}{2\tau^2 v_m} - \frac{H^4}{4\tau^4 v_m^3}\right)\Theta(\tau - H/v_m) \tag{41}$$

where Θ is the Heaviside step function

$$\begin{aligned} \Theta(x) &= 0 \qquad x < 0 \\ &= 1 \qquad x > 0 \end{aligned} \tag{42}$$

Note that $I(\tau)$ rises smoothly from 0 for $\tau \leq H/v_m$ to a maximum value of $3v_m/4$.

The shapes of $I(\tau)$ are similar for the two cases given; a sketch of $I(\tau)$ for a greatly attenuated spectrum is shown in figure 4.

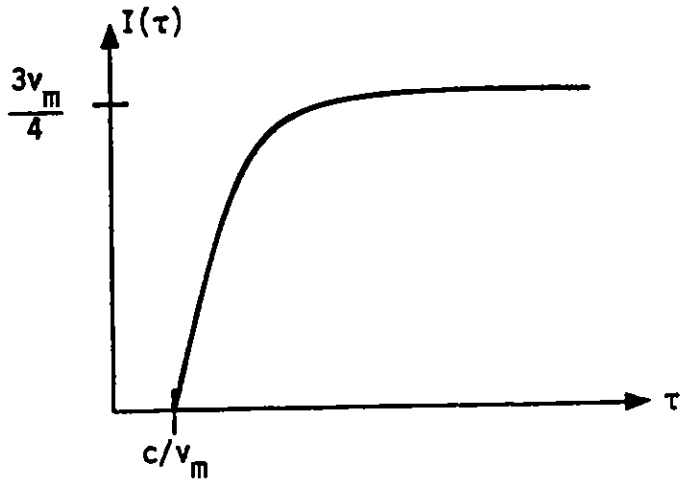

Figure 4. $I(\tau)$ for Monoenergetic Spectrum

SECTION III

EARLY TIME SURFACE MAGNETIC FIELDS

In this section we investigate the modification of the SGEMP response, that is the surface currents caused by the emission of photoelectrons from the surface materials, by an ambient plasma. To examine this modification we examine two cases; the first of these is a uniform plasma over a conducting surface. This plasma represents the plasma present about a missile surface at the time the X-rays are incident upon the surface; the electron density in this plasma is small compared to the surface electron density resulting from photoemission from the surface. The second case which we will consider is where the background plasma has a layer adjacent to the surface with a much higher electron density. This layer represents ions and their associated electrons which have been released from the surface by the breakdown of a dielectric coating over a conducting surface. The purpose of this second problem is to determine how magnetic fields created on the outside of the ion layer penetrate the layer to the conducting surface beneath; if the electron density of the plasma adjacent to the surface is much greater than the electron density of the emitted photoelectrons, the photoelectron currents will be balanced by plasma electron currents within the plasma, resulting in small electric fields in the plasma, and the space charge limiting of photoelectrons will occur outside the dense plasma layer.

1. UNIFORM PLASMA

To consider the first case, we focus on the magnetic field and solve for it by taking the curl of Ampere's law,

$$\nabla^2 B = \frac{1}{c^2} \frac{\partial^2 B}{\partial t^2} - \frac{4\pi}{c} \nabla \times (J_p + J_s) \tag{43}$$

Here, J_p is the current due to the photoemission, and J_s is the plasma (secondary) current. If we assume that the spatial extent of each electron's

trajectory is small, the curl of the plasma current is proportional to the magnetic field

$$\nabla \times J_s = \frac{-N_e e^2 B}{mc} \tag{44}$$

where N_e is the secondary electron density and m is the electron mass. (As noted in the introduction, we have ignored the magnetic forces on the electron in the derivation of equation (44) due to the small v_e/c and the long period of Larmor orbits compared to time scales of interest, which are <100 nsec.) Recalling that the plasma frequency is defined

$$\omega_p^2 = 4\pi N_e e^2/m \tag{45}$$

and substituting, we have

$$\nabla^2 B = \frac{1}{c^2}\left(\frac{\partial^2 B}{\partial t^2} + \omega_p^2 B\right) - \frac{4\pi}{c}(\nabla \times J_p) \tag{46}$$

If we have a situation so that the missile surface may be assumed to be a far-plane relative to the incoming X-ray wave fronts, it is valid to assume that $B = B_y$ and J_p are only functions of the distance from the surface z and the retarded time of the X-rays. They sweep along the surface with a phase velocity of $c/\sin\theta$ where θ is the angle of incidence of the X-rays. The X-ray retarded time τ is therefore defined

$$\tau = t - x \sin\theta/c \tag{47}$$

where the geometry is depicted in figure 5. With this our magnetic field equation is written

$$\frac{\partial^2 B}{\partial z^2} - \frac{\cos^2\theta}{c^2}\frac{\partial^2 B}{\partial \tau^2} - \left(\frac{\omega_p}{c}\right)^2 B = -\frac{4\pi}{c}\left(\frac{\sin\theta}{c}\frac{\partial J_{pz}}{\partial \tau} + \frac{\partial J_{px}}{\partial z}\right) \tag{48}$$

The left-hand side of this equation is just the wave equation for an elastically suspended string, and the right-hand side is the forcing function.

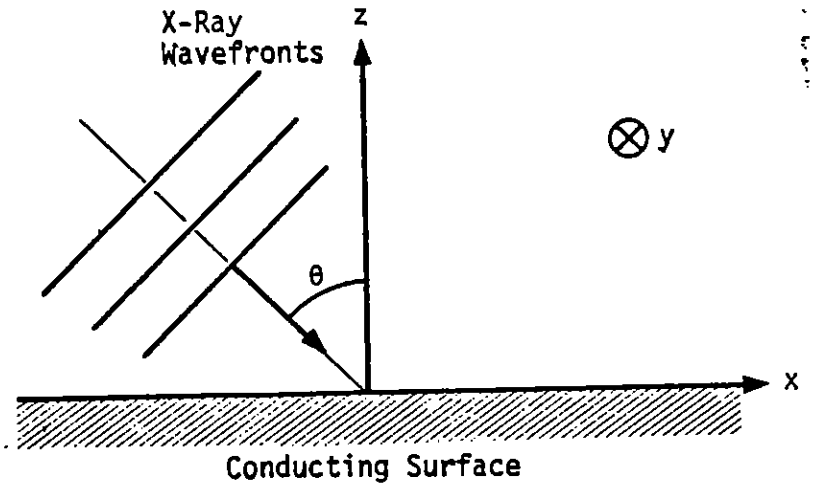

Figure 5. Far-plane Approximation for Missile Surface

The Green's function can be determined by Fourier transforming. The solution of the above equation for a simple harmonic wave moving away from a driving function at z = 0 is

$$B(\omega) = A(\omega)\left\{ \exp\left[-\sqrt{\frac{\omega_p^2}{\cos^2\theta} - \omega^2}\left(\frac{z\cos\theta}{c}\right) - i\omega t\right]\Theta(z) + \exp\left[+\sqrt{\frac{\omega_p^2}{\cos^2\theta} - \omega^2}\left(\frac{z\cos\theta}{c}\right) - i\omega t\right]\Theta(-z)\right\} \tag{49}$$

where Θ is the Heaviside step function as before. To obtain the Green's function we use a unit forcing function

$$\left.\frac{\partial B}{\partial z}\right|_{z\to 0^+} - \left.\frac{\partial B}{\partial z}\right|_{z\to 0^-} = 1 \tag{50}$$

and obtain

$$A(\omega) = \frac{c}{2\cos\theta}\left[\frac{\omega_p^2}{\cos^2\theta} - \omega^2\right]^{-1/2} \tag{51}$$

This may be transformed to the time domain by noting that $B(\omega)$ has essential singularities at $\omega = \pm \omega_b/\cos\theta$. In Fourier transforming to the time domain

$$G(z|t) = \frac{1}{2\pi}\int_{-\infty}^{\infty} d\omega\, B(z,\omega)\, e^{-i\omega t} \tag{52}$$

we must pick the integration contour as shown below (we can close the contour by an infinite semicircle through $\omega = i\infty$ for $ct < |z|\cos\theta$ and through $\omega = -i\infty$ for $ct > |z|\cos\theta$) so that $G(z|t) = 0$ for $t < 0$ (see figure 6). Note that the branch cut can be chosen to run between the essential singularities. For $ct > |z|\cos\theta$ we can collapse the contour about the branch cut and obtain for $z > 0$

$$G(z|t) = \frac{c}{2\cos\theta}\frac{1}{\pi}\int_{-a}^{a} d\omega\, \frac{e^{-i\omega t}\cos\left(ib\sqrt{a^2 - \omega^2}\right)}{\sqrt{a^2 - \omega^2}} \tag{53}$$

where $a = \omega_p/\cos\theta$ and $b = z\cos\theta/c$. Substituting $\omega = a\cos\phi$ we obtain

$$G(z|t) = \frac{c}{2\cos\theta}\frac{1}{\pi}\int_{0}^{\pi} d\phi\; e^{-iat\cos\phi}\cos(iab\sin\phi) \tag{54}$$

Substituting $\phi' = \phi - \cos^{-1} t/\sqrt{t^2 - b^2}$ (note that the arccosine is imaginary for real b as the argument is greater than one; here we can treat b as imaginary and analytically continue to real b as long as $b^2 < t^2$) we obtain

$$G(z|t) = \frac{c}{2\cos\theta}\frac{1}{2\pi}\int_{0}^{2\pi} d\phi'\, e^{ia\sqrt{t^2 - b^2}\cos\phi'} \tag{55}$$

$$= \frac{c}{2\cos\theta}\, J_0\left(a\sqrt{t^2 - b^2}\right)$$

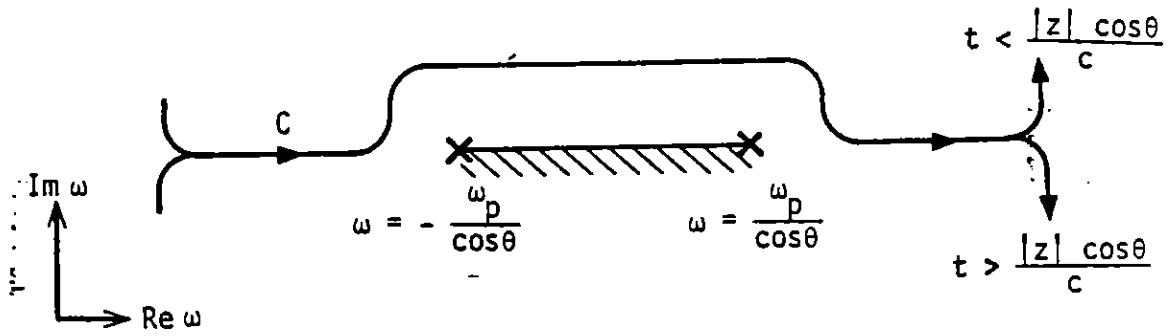

Figure 6. Integration Contour for G

The Green's function is

$$G(z|\tau) = \frac{c}{2\cos\theta} J_0\left(\frac{\omega_p}{\cos\theta}\sqrt{\tau^2 - \left(\frac{z\cos\theta}{c}\right)^2}\right)$$

$$\times [\theta(c\tau - z\cos\theta)\theta(z) + \theta(c\tau + z\cos\theta)\theta(-z)] \qquad (56)$$

where J_0 is the zeroth order Bessel function. The magnetic field is therefore given by

$$B(z,\tau) = 4\pi \int_{-\infty}^{\infty} dz' \int_0^{\tau} d\tau' G(z - z'|\tau - \tau')$$

$$\times \left[\frac{\sin\theta}{c^2}\frac{\partial J_{pz}}{\partial \tau'} + \frac{1}{c}\frac{\partial J_{px}}{\partial z'}\right] \qquad (57)$$

For the early-time response the currents in the x direction are negligible compared with those in the z direction. The air photocurrents have not yet had time to build up and there is no net emission current in the x direction. (The EM fields will induce currents in the x direction, but these are very small.) Further, the details of space-change-limiting are not sensitive to the ambient plasma. The density of emitted electrons is typically two to three orders of magnitude greater than the ambient plasma. The SGEMP boundary layer thickness is on the order of a few millimeters,

while the skin depth of the plasma c/ω_p is typically tens of centimeters. Under these conditions, the dynamics of the photoelectrons emitted from the surface may be assumed to be independent of the plasma dynamics and the solution for the magnetic field at the surface reduces to

$$B_s = \frac{4\pi\tan\theta}{c}\int_0^\tau \ddot{P}(\tau')\, J_0\left(\frac{\omega_p(\tau - \tau')}{\cos\theta}\right) d\tau' \tag{58}$$

where $\ddot{P}$ is the second time derivative of the dipole moment. (We have included the image sources.) $\dot{P}$ is related to J_{pz} by

$$\dot{P}(\tau) = \int_0^\infty J_{pz}(z,\tau)dz \tag{59}$$

One should note that this reduces to the vacuum case of Carron and Longmire (ref. 7), when the plasma density goes to zero so that $\omega_p = 0$

$$B_s = \frac{4\pi\tan\theta\ \dot{P}}{c} \tag{60}$$

The time history of $\dot{P}$ is determined by the dynamics of the space charge limiting of the photoelectrons emitted from the surface. This is not amenable to analytic calculation, but these dynamics (in vacuum) have been examined extensively by numerical methods in 1-D planar geometries (refs. 8 and 9). (These calculations are accurate when the space charge limiting distances are small compared to object radii of curvature, as they always are for X-ray fluences of interest to strategic missiles.) For the calculations shown in this section, we have assumed that the early part (< 1 ns) of the incident X-ray time history is a ramp, $f(t) = Rt$ for $t > 0$.

7. Carron, N. J. and C. L. Longmire, "Electromagnetic Pulse Produced by Obliquely Incident X-Rays," IEEE Trans. Nuc. Sci., NS-23, December 1976, pp. 1897-1902.
8. Longmire, C. L. and N. J. Carron, Scaling of the Time Dependent SGEMP Boundary Layer, DNA 3975T, Defense Nuclear Agency, April 1976.
9. Carron, N. J., Dynamical Solution of the SGEMP Electron Boundary Layer for Linearly Rising and Constant X-Ray Time Histories, DNA 4142T, Defense Nuclear Agency, December 1976.

Both the vacuum and plasma solutions show a tanθ dependence for the surface magnetic field. The plasma case additionally involves a convolution integral involving a Bessel function. The response will therefore depend on the relative magnitude of the time scales for establishing of the SGEMP boundary layer and the plasma's reaction to the fields. Longmire and Carron (ref. 8) noted the propensity of the Vlasov and Poisson equations to scaling and established characteristic units for the variables. The characteristic time, of course, depends critically on the assumed secular rise rate. It depends to a degree on the other parameters; blackbody temperature, fluence level, and electron yield of surface material. For the situation we have been considering, the X-rays have a linear rise and a typical characteristic time for establishing the SGEMP boundary layer is about 0.2 ns.

The response time of the plasma to the EM fields generated will have a characteristic time of $\omega_p/\cos\theta$. The $\cos\theta$ term results from the geometry of our problem. Monochromatic waves with frequencies higher than this will propagate, while lower frequency waves will be evanescent. These low frequencies are trapped near the surface with the result that the magnetic field persists long after the source is turned off. The Bessel function results in oscillations with an envelope with a late time behavior $t^{-\frac{1}{2}}$. A typical resulting surface current density is shown in figure 7.

We have also developed and implemented a simulation model to study the situation in detail. In this the photoelectrons are approximated as macroparticles and the plasma as a cold fluid. Although it contains somewhat more physical detail than the analytic model here outlined, it gives quite similar results.

2. PLASMA SHEATH

We next consider the case of a plasma with a step variation in density with a dipole source, resulting from the space charge limiting of photoelectrons ejected from the surface, occurring at the discontinuity.

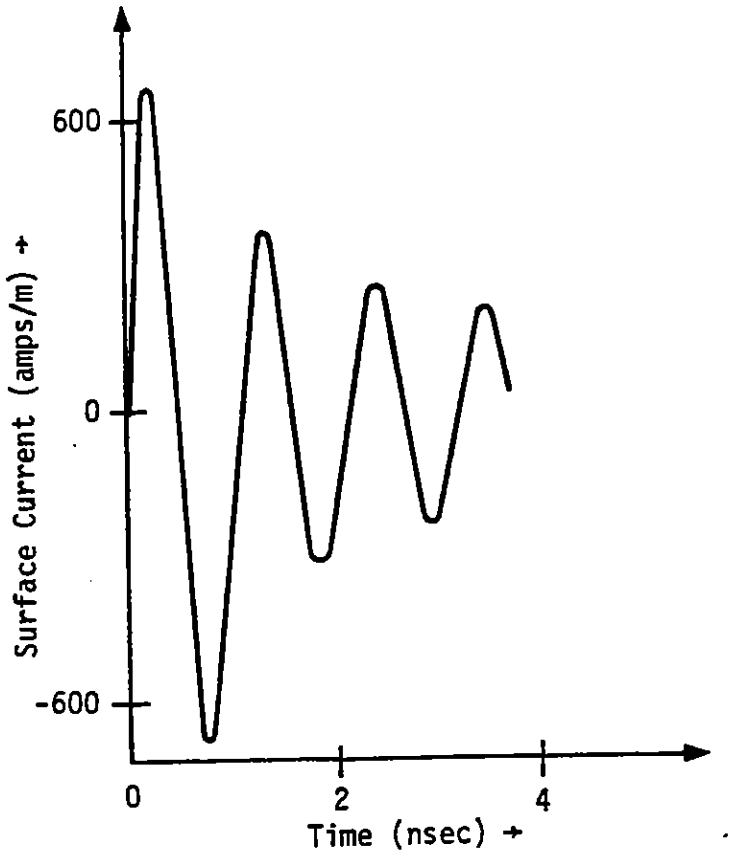

Figure 7. Surface Current Density

The purpose of this is to determine what densities of electron-ion plasma released from a surface *could* be important in modifying the surface magnetic field. At present there is no good theory for the quantity of ions released from an irradiated surface. The geometry we consider is shown in figure 8.

Primary photocurrents caused by the ejection of electrons from the surface exist in both plasma regions; the electrons do not space charge limit in the dense plasma region if this plasma density is much greater than the density of emitted electrons. Under these conditions the plasma currents nearly cancel the photocurrents so that the dominant driver of magnetic fields is the photocurrent in the sparse plasma region, which we calculate in this section.

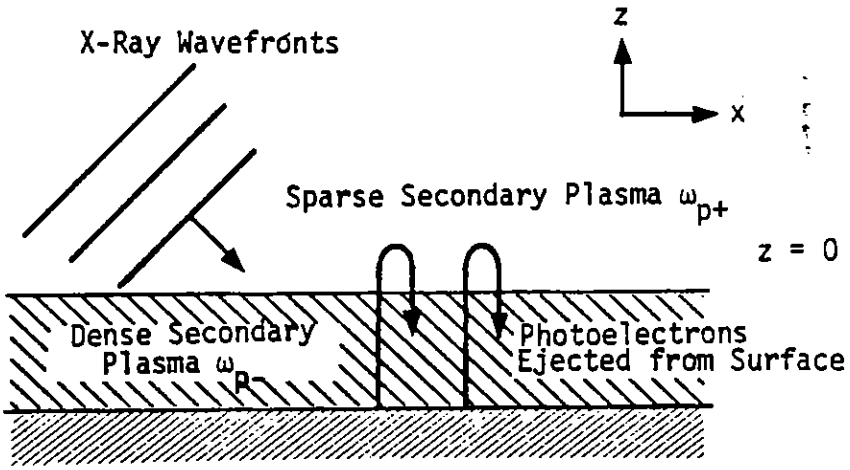

Figure 8. Plasma Sheath Geometry

The differences in plasma characteristics at this discontinuity will be modeled as a jump discontinuity in free-electron density and hence (according to equation (45)) a jump discontinuity in plasma frequency. Clearly, away from the interface (z = 0), the magnetic field satisfies

$$\left\{ \frac{\partial^2}{\partial z^2} - \frac{\cos^2\theta}{c^2} \frac{\partial^2}{\partial \tau^2} - \frac{\omega_{p\pm}^2}{c^2} \right\} B(z,\tau) = 0 \ , \text{ for } z \gtrless 0 \tag{61}$$

where ω_+ and ω_- are the plasma frequencies in the two plasmas. The plasma frequencies arise, as before, from the equation of motion of an electron in an electric field

$$\frac{dv}{dt} = - \frac{e}{m} E \tag{62}$$

hence, for a constant secondary electron density,

$$\frac{4\pi}{c} J_s = - \frac{4\pi}{c} N_e \, ev = \frac{\omega_p^2}{c} \int dt \, E \tag{63}$$

From the above expression, the boundary condition for the magnetic field at the interface may be determined. For early times, Ampefe's law has the form, for the transverse components,

$$-\frac{\partial}{\partial z} B = \frac{4\pi}{c} J_{sx} + \frac{1}{c}\frac{\partial}{\partial t} E_x = \frac{\omega_p^2}{c}\int dt\, E_x + \frac{1}{\partial t} E_x \tag{64}$$

Fourier transforming time, $t \to \omega$, yields

$$-\frac{\partial}{\partial z} B = \left(\frac{\omega_p^2}{i\omega c} + \frac{i\omega}{c}\right) E_x \tag{65}$$

hence the boundary condition at the interface utilizing the continuity of the electromagnetic fields gives

$$B\Big|_{z=0_+} = B\Big|_{z=0_-} \tag{66}$$

and

$$\frac{1}{\omega_{p+}^2 - \omega^2}\ \frac{\partial}{\partial z} B\Big|_{z=0_+} = \frac{1}{\omega_{p-}^2 - \omega^2}\ \frac{\partial}{\partial z} B\Big|_{z=0_-} \tag{67}$$

The jump discontinuity in the derivative at the density discontinuity is

$$\frac{\partial}{\partial z} B\Big|_{z=0_+} - \frac{\partial}{\partial z} B\Big|_{z=0_-} = \frac{\omega_{p+}^2 - \omega_{p-}^2}{\omega_{p+}^2 - \omega^2} B\Big|_{z=0_+}$$

$$= \frac{\omega_{p+}^2 - \omega_{p-}^2}{\omega_{p-}^2 - \omega^2}\frac{\partial}{\partial z} B\Big|_{z=0_-} \tag{68}$$

which may then be directly incorporated into the general, Fourier transformed differential equation including the dipole photocurrent driver normal to the interface in the sparse plasma region,

$$\left\{\frac{\partial^2 B}{\partial z^2} + \frac{\cos^2\theta}{c^2}\,\omega^2 B - \frac{\omega_{p\pm}^2}{c^2}\,B - \frac{\omega_{p+}^2 - \omega_{p-}^2}{\omega_{p+}^2 - \omega^2}\,\frac{\partial B}{\partial z}\Big|_{z=0_+}\,\delta(z)\right\}$$

$$= \frac{4\pi\sin\theta}{c^2}\, i\omega J_{pz}(\omega)\,\delta[z] \tag{69}$$

By direct substitution, the magnetic field which satisfies this equation can be seen to be

$$B(z,\omega) = \frac{4\pi\sin\theta}{c^2}\, i\omega\, J_{pz}(\omega)\, \exp[\pm\Gamma_\pm z] \Big/ \left\{\Gamma_+ + \frac{\omega_{p+}^2 - \omega^2}{\omega_{p-}^2 - \omega^2}\,\Gamma_-\right\} \tag{70}$$

$$\text{for } z \gtrless 0$$

$$\Gamma_\pm = \frac{\sqrt{\omega_{p\pm}^2 - \omega^2\cos^2\theta}}{c} \tag{71}$$

The inverse Fourier transform of the above expression is not easy; therefore, we shall consider the special case where

$$\omega_{p-}^2 >> \omega_{p+}^2 \tag{72}$$

and the contributions of the high frequency components to the above expression are small, e.g.,

$$J_{pz}(\omega) \approx 0 \quad \text{for } \omega \gtrsim \omega_{p-} \tag{73}$$

For such a case,

$$B(z,\omega) = \frac{4\pi i\sin\theta}{c^2}\,\omega J_{pz}(\omega)\,\frac{\exp[\pm\Gamma_\pm z]}{\Gamma_+} \qquad \text{for } z \gtrless 0 \tag{74}$$

In the low frequency plasma ($z > 0$), this is identical to the single plasma result, equation (57)

$$B(z,\tau) = \frac{4\pi\tan\theta}{c}\int_0^\tau d\tau' \frac{\partial}{\partial\tau} J_{pz}(\tau - \tau') J_o\left(\frac{\omega_{p+}}{\cos\theta}\sqrt{\tau'^2 - \frac{z^2\cos^2\theta}{c^2}}\right) \quad (75)$$

and in the dense plasma, ($z < 0$), we find (ref. 10), for small z,

$$B(z,\tau) = \frac{4\pi\tan\theta}{c}\int_0^\tau d\tau' \frac{\partial}{\partial\tau} J_{pz}(\tau - \tau') J_o(\omega_{p+}\tau') \exp[\omega_{p-}z/c] \quad (76)$$

The physical significance of this solution is that it gives us an indication of what densities and layer thicknesses of plasma released from a dielectric surface are important in shielding the surface from magnetic fields created outside this layer of dielectric. Specifically, this effect becomes important if the layer is thicker than

$$\ell > \frac{c}{\omega_p} \quad (77)$$

where ω_p is calculated with the electron density in the layer itself.

10. Abramowitz, M. and I. A. Stegun, Handbook of Mathematical Functions, U. S. Government Printing Office, 1970.

SECTION IV

LATE-TIME SOLUTIONS

In this section we investigate the surface electric and magnetic fields caused by the motion of photoelectrons created in the air. This mechanism is analogous to the usual close-in coupling with gamma rays; the greatest magnitude of this coupling should be seen when the X-rays are parallel to the conducting surface. We will first examine the fields seen in a uniform collisionless plasma with constant density. We will next separately examine the effects of a time-varying density and electron-neutral collisions in the plasma; the physics of these effects can be seen separately and the mathematics of treating them together appears to be intractable. Finally we will examine the effects of a surface layer with a high electron density on the surface magnetic fields.

1. BASIC SOLUTION

We first consider the case with a constant density and no collisions. Maxwell's equations are

$$\nabla \times B = \frac{1}{c}\frac{\partial E}{\partial t} + \frac{4\pi}{c} J_p + \frac{4\pi}{c} J_s \tag{78}$$

and

$$\nabla \times E = -\frac{1}{c}\frac{\partial B}{\partial t} \tag{79}$$

where our frame is as before (figure 5) except that we fix $\theta = 90°$. Taking the curl of B as before

$$\nabla^2 B = \frac{1}{c^2}\frac{\partial^2 B}{\partial t^2} - \frac{4\pi}{c}(\nabla \times J_p) - \frac{4\pi}{c}(\nabla \times J_s) \tag{80}$$

and using the fact that, for X-rays incident parallel to the surface

$$\frac{\partial}{\partial x} = -\frac{1}{c}\frac{\partial}{\partial t} \tag{81}$$

we obtain

$$\frac{\partial^2 B}{\partial z^2} = -\frac{4\pi}{c}\left\{\frac{\partial J_{px}}{\partial z} + \frac{1}{c}\frac{\partial J_{pz}}{\partial t}\right\} - \frac{4\pi}{c}\left\{\frac{\partial J_{sx}}{\partial z} + \frac{1}{c}\frac{\partial J_{sz}}{\partial t}\right\} \tag{82}$$

From the z component of Ampere's law we obtain

$$\frac{\partial B}{\partial x} = \frac{1}{c}\frac{\partial E_z}{\partial t} + \frac{4\pi}{c}(J_{pz} + J_{sz}) \tag{83}$$

Using our retarded frame and, for convenience, $G = E_z + B$

$$\frac{\partial G}{\partial t} = -4\pi\,(J_{pz} + J_{sz}) \tag{84}$$

Finally from the $\nabla \times E$ equation

$$\frac{\partial E_x}{\partial z} = -\frac{1}{c}\frac{\partial G}{\partial t} = \frac{4\pi}{c}(J_{pz} + J_{sz}) \tag{85}$$

For the secondary electrons

$$\frac{\partial J_{sz}}{\partial t} = \frac{e^2 N_e}{m}(G - B) \tag{86}$$

$$\frac{\partial J_{sx}}{\partial t} = \frac{e^2 N_e}{m} E_x \tag{87}$$

A bit of substitution yields for B

$$\frac{\partial^2 B}{\partial z^2} - \frac{\omega_p^2}{c^2} B = -\frac{4\pi}{c}\left(\frac{\partial J_{px}}{\partial z} + \frac{1}{c}\frac{\partial J_{pz}}{\partial t}\right) \tag{88}$$

which has the solution

$$B = \frac{2\pi}{\omega_p} \int_{-\infty}^{\infty} dz' \, e^{-|z-z'|\omega_p/c} \left[\frac{\partial J_{px}}{\partial z'} + \frac{1}{c} \frac{\partial J_{pz}}{\partial t} \right] \tag{89}$$

We next consider the relative importance of the two source terms and how one includes the conducting surface. Introducing the conductor is most easily done with image currents (see figure 9), so that if J_{px} is spatially uniform above the conductor, the relevant derivative is

$$\frac{\partial J_{px}}{\partial z} = 2\delta(z) J_{px} \tag{90}$$

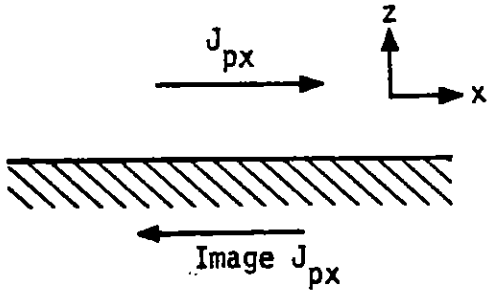

Figure 9. Introduction of a Conductor Using Image Currents

If $\frac{\partial J_{pz}}{\partial t} << \omega_p J_{px}$, as it almost always is in cases of interest, J_{px} is the dominant driver of late time near-surface magnetic fields and

$$B(z,t) = \frac{4\pi}{\omega_p} J_{px}(t) \, e^{-z\omega_p/c} \tag{91}$$

We can find the differential equation for G

$$\frac{\partial^2 G}{\partial t^2} + \omega_p{}^2 G = + \omega_p{}^2 B - 4\pi \frac{\partial J_{pz}}{\partial t} \tag{92}$$

which has the solution

$$G(z,t) = + \frac{1}{\omega_p} \int_0^t dt' \sin \omega_p(t-t') \left\{ \omega_p^2 \, B(z,t') - 4\pi \frac{\partial J_{pz}}{\partial t'} \right\} \qquad (93)$$

or, with J_{px} as above and neglecting J_{pz} near the surface,

$$G = +4\pi \, e^{-z\omega_p/c} \int_0^t dt' \sin \omega_p(t-t') \, J_{px}(t') \qquad (94)$$

We can now solve for J_{sz}

$$J_{sz} = - \frac{1}{4\pi} \frac{\partial G}{\partial t} - J_{pz} \qquad (95)$$

which allows us to solve for E_x

$$E_x = \int_0^z dz' \frac{4\pi}{c} (J_{pz} + J_{sz}) = - \frac{1}{c} \int_0^z dz' \frac{\partial G(z',t)}{\partial t} \qquad (96)$$

or, again in the approximation of small J_{pz} and uniform J_{px}

$$E_x = -4\pi \left(1 - e^{-z\omega_p/c} \right) \int_0^t dt' \cos \omega_p(t-t') \, J_{px}(t') \qquad (97)$$

This solution is for a spatially uniform, time independent plasma density. The numerical results discussed below indicate that even for the long time periods the convection of plasma density will produce small gradients. The plasma density will build up on a slow time scale due to slowing down of primary electrons. This solution also requires knowledge of the photocurrents. A preliminary estimate of the photocurrents can be made by using the method of O'Dell, Longmire, and Higgins (ref. 11),

11. Higgins, D. F., C. L. Longmire and A. A. O'Dell, A Method for Estimating the X-ray Produced Electromagnetic Pulse Observed in the Source Region of a High Altitude Burst, DNA 3218T, Defense Nuclear Agency, November 1973.

and forcing the radial electric field to vanish near the surface with a characteristic length c/ω_p, where ω_p is the time dependent plasma frequency. (This method was used in an earlier report.*) A representative surface current density due to this effect is shown in figure 10.

To obtain more complete estimates we have developed a computer code which calculates the self-consistent fields and currents for our situation. We assume both the air photoelectrons and secondary electrons may be approximated by the cold fluid equations. For low energies (< 20 keV) photoelectrons have a velocity distribution which is strongly peaked in the transverse direction, in the direction of the incident photon electric field. In a uniform medium these currents from adjacent volume elements will cancel due to symmetry. Near the metal surface, however, there will be a strong transverse current source after the end of the photon pulse and we have approximated this source in our numerical model.

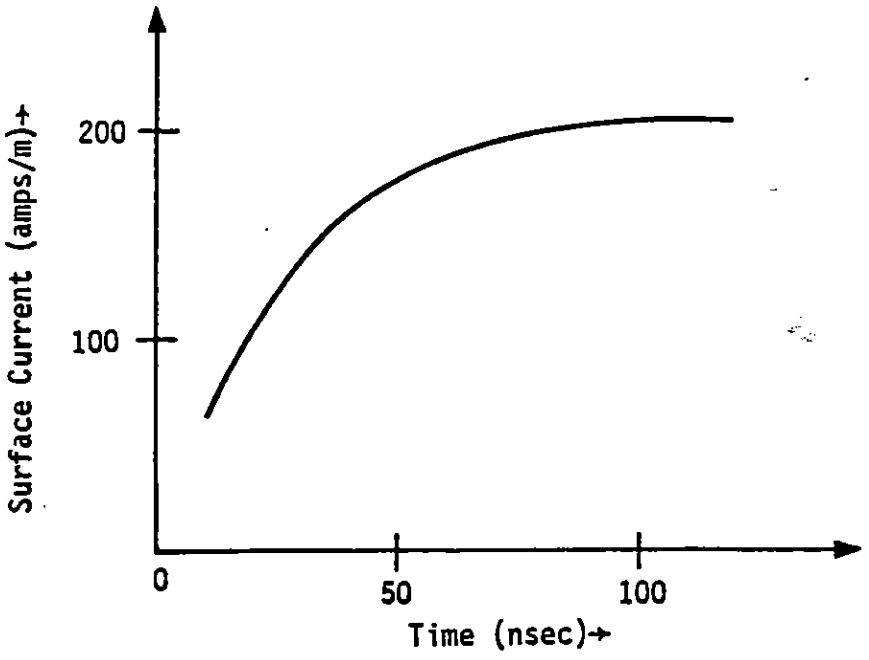

Figure 10. Typical Late Time Surface Current Density

*Gilbert, J. L., W. E. Hobbs and H. J. Price (to be published).

2. TIME VARYING PLASMA DENSITY

We now proceed to allowing the density to vary with time. We will show that there will be a small perturbation to B which oscillates at the plasma frequency, unlike the solution for a time independent plasma. Unfortunately, in this regime the time and distance dependences are coupled, and the resulting equations must be solved numerically.

We will assume that the plasma density varies much more slowly than the other variables, specifically, we require that

$$\frac{\ddot{\omega}_p}{\omega_p} \text{ and } \left(\frac{\dot{\omega}_p}{\omega_p}\right)^2 \ll \omega_p^2 \tag{98}$$

In cases of interest the left-hand side of (98) is typically 10^{17} sec^{-2} and the right is 10^{18} sec^{-2}. Then defining

$$h(t) = \frac{\partial}{\partial t} \ell n(N_e(t)) \tag{99}$$

and

$$G(t,z) = E_z(t,z) + B(t,z) \tag{100}$$

for notational convenience, the problem is governed by the same five equations as before, where $J_p = J_{px}$, $J_x = J_{sx}$ and $J_z = J_{sz}$.

$$\frac{\partial^2 B}{\partial z^2} = -\frac{4\pi}{c}\left\{\frac{\partial J_x}{\partial z} + \frac{1}{c}\frac{\partial J_z}{\partial t}\right\} - \frac{4\pi}{c}\frac{\partial J_p}{\partial z} \tag{101}$$

$$\frac{\partial E_x}{\partial z} = \frac{4\pi}{c} J_z \tag{102}$$

$$\frac{\partial G}{\partial t} = -4\pi J_z \tag{103}$$

$$\frac{\partial J_z}{\partial t} = \frac{N_e e^2}{m} (G - B) \tag{104}$$

$$\frac{\partial J_x}{\partial t} = \frac{N_e e^2}{m} E_x \tag{105}$$

Taking the time derivative of equation (101), and substituting, we have,

$$\frac{\partial^3 B}{\partial z^2 \partial t} = - \frac{4\pi}{c} \left\{ \frac{N_e e^2}{m} \frac{\partial E_x}{\partial z} + \frac{1}{c} \frac{\partial}{\partial t} \left[\frac{N_e e^2}{m} (G - B) \right] \right\} - \frac{4\pi}{c} \frac{\partial^2 J_p}{\partial z \partial t} \tag{106}$$

$$= - \frac{4\pi}{c} \left\{ \frac{\omega_p^2}{c} J_z + \frac{\omega_p^2}{4\pi c} h(t)(G-B) - \frac{\omega_p^2}{c} J_z - \frac{\omega_p^2}{4\pi c} \frac{\partial B}{\partial t} \right\}$$

$$- \frac{4\pi}{c} \frac{\partial^2 J_p}{\partial z \partial t}$$

Collecting terms and integrating in time the equation reduces to

$$\frac{\partial^2 B}{\partial z^2} - \frac{\omega_p^2}{c^2} B = - \int dt \, \frac{\omega_p^2}{c^2} h(t) G - \frac{4\pi}{c} \frac{\partial J_p}{\partial z} \tag{107}$$

To close the system of equations (assuming that the plasma density and photocurrent are given), we differentiate and eliminate J_{sz} to get

$$\frac{\partial^2 G}{\partial t^2} = - \omega_p^2 (G - B) \tag{108}$$

For small h, the first term on the right in equation (107) will be much smaller than the other terms (which all appeared in the solution for the constant density problem), so the natural modification is to let

$$B = B_L + B_s \tag{109}$$

and rewrite equations (107) and (108) as three equations

$$\left(\frac{\partial^2}{\partial z^2} - \frac{\omega_p^2}{c^2}\right) B_L = -\frac{4\pi}{c}\frac{\partial J_p}{\partial z} \tag{110}$$

$$\left(\frac{\partial^2}{\partial t^2} + \omega_p^2\right) G = \omega_p^2 B_L \tag{111}$$

$$\left(\frac{\partial^2}{\partial z^2} - \frac{\omega_p^2}{c^2}\right) B_s = \int dt\, \frac{\omega_p^2}{c^2} h(t) G \tag{112}$$

Now the solution to equation (110) will be the same as for B in the constant density case. If $J_p = f(t)\{\Theta(z) - \Theta(-z)\}$ we have

$$B_L = \frac{4\pi}{\omega_p} f(t)\, e^{-|z|\omega_p/c} \tag{113}$$

Now however, equation (111) for G cannot be solved exactly, and we instead use a WKB approximation to handle the homogeneous equation. As a first cut we choose

$$G_o = e^{-i\int_o^t \omega_p(t')dt'} \tag{114}$$

which yields

$$\left(\frac{\partial^2}{\partial t^2} + \omega_p^2\right) G_o = -i\dot{\omega}_p G_o \tag{115}$$

Introducing a perturbation to improve the approximation, we have

$$G_1 = e^{-i\int_o^t (\omega_p(t') + \omega_1(t'))dt'} \tag{116}$$

so that

$$\left(\frac{\partial^2}{\partial t^2} + \omega_p^2\right)G_1 = (-2\omega_p\omega_1 - \omega_1^2 - i\dot{\omega}_p - i\dot{\omega}_1)G_1 \tag{117}$$

If ω_1 is chosen so that

$$2\omega_p\omega_1 = -i\dot{\omega}_p \tag{118}$$

then we may solve for G_1 and obtain

$$G_1 = \frac{1}{\sqrt{\omega_p(t)}}\, e^{-i\int_0^t \omega_p(t')\, dt'} \tag{119}$$

which will satisfy the homogeneous part of equation (111) to the first order in the approximations on $\dot{\omega}_p$ and $\dot{\omega}_p$.

From this we need to construct a Green's function for equation (111); following the form of the solution for the time independent case we write

$$G_G = \frac{g(t')}{\sqrt{\omega_p(t)}} \sin\left(\int_{t'}^{t} \omega_p(\tau)d\tau\right) \tag{120}$$

and solve for $g(t')$ in equation (111). This yields

$$G_G(t,t') = \frac{1}{\sqrt{\omega_p(t)\omega_p(t')}} \sin\left(\int_{t'}^{t} \omega_p(\tau)d\tau\right) \tag{121}$$

so that the solution for G will be

$$G(t,z) = \frac{4\pi}{\sqrt{\omega_p(t)}} \int_0^t \sqrt{\omega_p(t')}\, f(t')\, e^{-\frac{|z|}{c}\omega_p(t')} \sin\left(\int_{t'}^{t} \omega_p(\tau)d\tau\right)dt' \tag{122}$$

We are now in a position to solve for B_s, the correction to B due to the time dependence of the plasma. The Green's function for B_s will be

$$B_G = -\frac{c}{2\omega_p} e^{-\frac{\omega_p}{c}|z - z'|} \tag{123}$$

and this produces a solution

$$B_s = \frac{4\pi}{\omega_p(t)} \int_0^t dt' \, \omega_p^{3/2}(t') h(t') \int_0^{t'} dt'' \sqrt{\omega_p(t'')} f(t'') \sin\left(\int_{t''}^{t'} \omega_p(\tau) d\tau\right) \tag{124}$$

$$\times \frac{\omega_p(t'') \, e^{-\omega_p(t)z/c} - \omega_p(t) \, e^{-\omega_p(t'')z/c}}{\omega_p^2(t) - \omega_p^2(t'')}$$

The electric fields can now be determined, although numerical integration is required.

$$E_z = G - B$$

$$= \frac{4\pi}{\sqrt{\omega_p(t)}} \int_0^t \sqrt{\omega_p(t')} \, f(t') \, e^{-\frac{z\omega_p(t')}{c}} \sin\left(\int_{t'}^t \omega_p(\tau) d\tau\right)$$

$$- \frac{4\pi}{\omega_p} f(t) \, e^{-\frac{z\omega_p(t)}{c}} - B_s \tag{125}$$

An equation for E_x may be derived from the Ampere and Faraday laws in retarded time, and the equation of motion for a particle

$$\frac{\partial E_x}{\partial z} = \frac{4\pi}{c} J_z = \int \frac{\omega_p^2}{c} (G - B) dt' \tag{126}$$

Thus

$$E_x = \int_0^z dz' \int_0^t \frac{\omega_p^2(t')}{c} E_z(t')dt' \qquad (127)$$

The relevant fact to note from this solution with a spatially uniform time varying plasma is that the magnetic field has a small part, of order $\frac{1}{\omega_p}\frac{d}{dt}(\log N_e)$, which oscillates at the plasma frequency. The previous solution with N_e held fixed had no high frequency components to B and the surface magnetic field was simply proportional to the time integral of the X-ray pulse. In both cases we observe high frequency oscillations in the normal electric field and in the electric field parallel to the surface away from the surface.

3. COLLISIONAL DAMPING

We return now to the case of a time independent, spatially uniform plasma over a conductor, to investigate the effects of a damping term in the equation for the secondary electron current. Unlike the time dependent plasma case, the derivation of an integral solution for B requires no further approximations, and as may be expected, the oscillations in B disappear.

The behavior of the plasma is now governed by equations (101), (102), and (103) of the previous section, and the following two equations for the secondary current.

$$\frac{\partial J_z}{\partial t} = \frac{\omega_p^2}{4\pi}(G - B) - \nu J_z \qquad (128)$$

$$\frac{\partial J_x}{\partial t} = \frac{\omega_p^2}{4\pi} E_x - \nu J_x \qquad (129)$$

To obtain an equation for B, first differentiate equation (129) by z to obtain

$$\frac{\partial^2 J_x}{\partial t \partial z} = \frac{\omega_p^2}{4\pi} \frac{\partial E_x}{\partial z} - \nu \frac{\partial J_x}{\partial z} \tag{130}$$

which can be substituted into equation (101) of the previous section after taking the time derivative of the latter.

$$\frac{\partial^3 B}{\partial z^2 \partial t} = - \frac{4\pi}{c} \left\{ \frac{\partial^2 J_x}{\partial z \partial t} + \frac{1}{c} \frac{\partial^2 J_z}{\partial t^2} \right\} - \frac{4\pi}{c} \frac{\partial^2 J_p}{\partial z \partial t} \tag{131}$$

After substituting for $\partial^2 J_x / \partial z \partial t$ from equation (130) and for $\partial^2 J_z / \partial t^2$ from equation (128), we have

$$\frac{\partial^2 \dot{B}}{\partial z^2} = - \frac{4\pi}{c} \left\{ \frac{\omega_p^2}{c} J_z + \frac{\omega_p^2}{4\pi c} (\dot{G} - \dot{B}) \right\} - \frac{4\pi}{c} \frac{\partial \dot{J}_p}{\partial z}$$

$$+ \frac{4\pi\nu}{c} \left\{ \frac{\partial J_x}{\partial z} + \frac{1}{c} j_z \right\} \tag{132}$$

The last term in brackets may be eliminated by substituting from equation (104) of the previous section, while the time derivative of G will cancel the J_{sz} term inside the first bracket. Thus our equation for B is

$$\left(\frac{\partial^2}{\partial z^2} - \frac{\omega_p^2}{c^2} \right) \dot{B} + \nu \frac{\partial^2}{\partial z^2} B = - \frac{4\pi}{c} \frac{\partial}{\partial z} (\dot{j}_p + \nu J_p) \tag{133}$$

which for notational convenience we write as

$$\left(\frac{\partial^2}{\partial z^2} - k_p^2 \right) \dot{B} + \nu \frac{\partial^2 B}{\partial z^2} = \frac{8\pi}{c} \delta(z) \, F(t) \tag{134}$$

since the photocurrent is homogeneous for $z > 0$, and matched by an image current beneath the surface of the conductor.

To derive the Green's function, first transform equation (134) in time to give, with a time delta function driver, $4F(t)/c = \delta(t)$

$$(-i\omega + \nu)\frac{\partial^2}{\partial z^2} B + i\omega k_p^2 B = \delta(z) \tag{135}$$

This equation has the same general solution in z as the equation for B in the time independent, undamped current case, so solving for coefficients we have

$$B(\omega,z) = \frac{1}{2k_p} \frac{e^{-k_p z\sqrt{\frac{-i\omega}{-i\omega+\nu}}}}{\sqrt{(-i\omega)(-i\omega+\nu)}} \tag{136}$$

Note that we have essential singularities at $\omega = 0$ and $\omega = -i\nu$, but the branch cut of the function can be run between them as we do not have an essential singularity at infinity. As noted in the last section the path of integration should be taken as shown in figure 11 so that $B = 0$ for $t < 0$ and the contours can be closed with semicircles at infinity as shown.

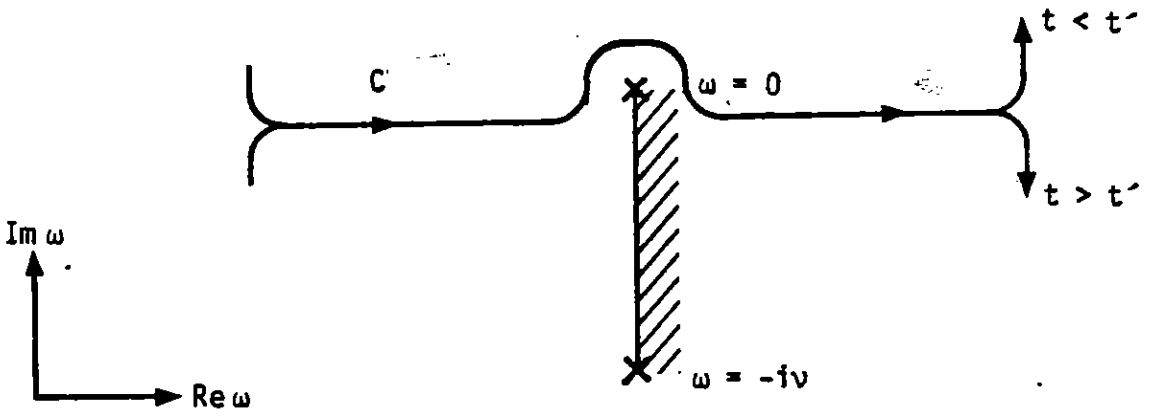

Figure 11. Integration Contour for B

For $t > t'$, the integral may be shrunk down to the branch cut and rewritten as

$$B(t - t') = \frac{-\Theta(t - t')}{k_p} \int_0^\nu \frac{e^{-\lambda(t-t')} \cos\left(k_p z \sqrt{\frac{\lambda}{\nu-\lambda}}\right)}{\sqrt{\lambda(\nu - \lambda)}} \, d\lambda \qquad (137)$$

since the exponential term may be kept on the part of the branch where it is bounded, and the contributions at the endpoints will vanish. The solution for equation (134) is then

$$B(t,z) = \frac{4}{\omega_p} \int_0^t dt\, F(t') \int_0^\nu e^{-\lambda(t-t')} \frac{\cos\left(k_p z \sqrt{\frac{\lambda}{\nu-\lambda}}\right)}{\sqrt{\lambda(\nu - \lambda)}} \, d\lambda \qquad (138)$$

Since the electric fields may be expressed simply in terms of the perpendicular current, let us solve for it before dealing with the fields. The equation governing it may be obtained by differentiating equation (128) and substituting for $\dot{G}$ from the previous section, so that

$$\left(\frac{\partial^2}{\partial t^2} + \nu \frac{\partial}{\partial t} + \omega_p^2\right) J_z = - \frac{\omega_p^2}{4\pi} \dot{B} \qquad (139)$$

By Fourier transforming the left side of equation (139) and inverse transforming the resulting equation, we obtain the Green's function for J,

$$J_G = \frac{1}{2\pi} \int_{-\infty}^{\infty} \frac{e^{-i\omega(t-t')} d\omega}{\omega^2 + i\nu\omega - \omega_p^2} \qquad (140)$$

This may be evaluated by closing the contour and evaluating residues, but the contour must go above the ω axis for $t < t'$ and below the axis for $t > t'$.

Thus $J_G = 0$ for $t < t'$ since both poles lie below the ω axis (assuming $\omega_p > \nu/2 > 0$). Denoting the poles as ω_1 and ω_2, where

$$\omega_1 = \frac{-i\nu + \sqrt{4\omega_p^2 - \nu^2}}{2} \tag{141}$$

and

$$\omega_2 = \frac{-i\nu - \sqrt{4\omega_p^2 - \nu^2}}{2} \tag{142}$$

the equation for J_G will be

$$J_G = -i\left\{\frac{e^{-i\omega_1(t-t')}}{(\omega_1 - \omega_2)} + \frac{e^{-i\omega_2(t-t')}}{(\omega_2 - \omega_1)}\right\}$$

$$= \frac{2}{\sqrt{4\omega_p^2 - \nu^2}}\, e^{-\frac{\nu}{2}(t-t')} \sin\left(\frac{\sqrt{4\omega_p^2 - \nu^2}}{2}\,(t - t')\right) \tag{143}$$

To simplify notation, let

$$\omega_o = \sqrt{\frac{4\omega_p^2 - \nu^2}{2}} \tag{144}$$

so that

$$J_G = \frac{1}{\omega_o}\, e^{-\frac{\nu}{2}(t-t')} \sin \omega_o(t - t') \tag{145}$$

To complete the solution, note that

$$\dot{B} = \frac{4}{\omega_p}\left[F(t)\int_0^{\nu} \frac{\cos\left(k_p z \sqrt{\frac{\lambda}{\nu-\lambda}}\right)}{\lambda(\nu-\lambda)}\, d\lambda\right.$$

$$- \int_0^t F(t') \int_0^\nu e^{-\lambda(t-t')} \cos\left(k_p z \sqrt{\frac{\lambda}{\nu-\lambda}}\right) \sqrt{\frac{\lambda}{\nu-\lambda}}\, d\lambda\, dt' \Bigg]$$

$$= \frac{4}{\omega_p}\left[\pi e^{-k_p|z|} F(t) - \int_0^t F(t') \int_0^\nu e^{-\lambda(t-t')} \cos\left(k_p z \sqrt{\frac{\lambda}{\nu-\lambda}}\right) \sqrt{\frac{\lambda}{\nu-\lambda}}\, d\lambda dt'\right] \tag{146}$$

and for convenience, denote the term in brackets as $\Gamma(t,z)$. Then

$$J_{sz}(t,z) = \frac{\omega_p}{\pi\omega_o} \int_0^t dt'\, e^{-\frac{\nu}{2}(t-t')} \sin\omega_o(t-t')\Gamma(t',z) \tag{147}$$

Recall that $E_z = G - B$, so that we may use equation (128) and (147) to solve for E_z

$$E_z = \frac{4\pi}{\omega_p^2}\left(\dot{J}_{sz} + \nu J_{sz}\right)$$

$$= \frac{4}{\omega_p \omega_o}\left[\int_0^t e^{-\frac{\nu}{2}(t-t')}\left(\frac{\nu}{2}\sin\omega_o(t-t') + \omega_o \cos\omega_o(t-t')\right)\Gamma(t',z)dt'\right] \tag{148}$$

To evaluate E_x we use equation (102) and write

$$E_x = \frac{4\pi}{c}\int_0^z dz'\, J_{sz}$$

$$= \frac{4}{c}\frac{\omega_p}{\omega_o}\int_0^t dt'\, e^{-\frac{\nu}{2}(t-t')} \sin\omega_o(t-t') \int_0^z dz' \Gamma(t',z') \tag{149}$$

There are two relevant points worth learning from this calculation; the first is that the oscillatory electric fields decay as $e^{-\nu t/2}$ after the end of the X-ray pulse, but that the magnetic field arising from the $\lambda \to 0$ portion of the integration in equation (138) decays slowly. The second point can be seen directly from equation (136); whereas the magnetic fields in the basic solution decreased exponentially in space with a distance scale $1/k_p$, the low frequency ($|\omega| \ll \nu$) fields in the dissipative plasma fall off more slowly. This process is the same as the diffusion of magnetic fields through an imperfect conductor.

The result of this is that the presence of damping does not cause the late time magnetic field shown in figure 9 to fall off at the end of the X-ray pulse as one might expect.

4. DENSE PLASMA BOUNDARY LAYER

We examine a time independent, collisionless plasma with a density discontinuity at z = 0 as in the last section. Away from the interface at z = 0 the magnetic field satisfies

$$\left[\frac{\partial^2}{\partial z^2} - \frac{\omega_{p\pm}^2}{c^2}\right] B(z) = 0 \qquad \text{for } z \gtrless 0 \tag{150}$$

Ampere's law at the interface of the plasmas, then, is taken to manifest the transverse current driver,

$$-\frac{\partial}{\partial z} B = \frac{4\pi}{c} J_{px} + \left(\frac{i\omega}{c} + \frac{\omega_{p\pm}^2}{i\omega c}\right) E_x \tag{151}$$

The appropriate boundary condition at the interface then becomes

$$\left(1 - \frac{\omega_{p+}^2}{\omega^2}\right)^{-1}\left[\frac{\partial}{\partial z} B\Big|_{z=0_+} + \frac{4\pi}{c} J_{px}\right] = \left(1 - \frac{\omega_{p-}^2}{\omega^2}\right)^{-1}\left[\frac{\partial}{\partial z} B\Big|_{z=0_-} + \frac{4\pi}{c} J_{px}\right] \tag{152}$$

or

$$\frac{\partial}{\partial z} B\Big|_{z=0_+} - \frac{\partial}{\partial z} B\Big|_{z=0_-} = \left[\frac{\omega_{p+}^2 - \omega_{p-}^2}{-\omega^2 + \omega_{p-}^2}\right]\left[\frac{\partial}{\partial z} B\Big|_{z=0_-} + \frac{4\pi}{c} J_{px}\right] \tag{153}$$

Utilizing the continuity of the magnetic field then yields,

$$B = -4\pi J_{px} \frac{\omega_{p+} - \omega_{p-}}{\omega_{p+}\omega_{p-}} \exp\left[-\omega_{p\pm}|z|\Big/c\right] \qquad \text{for } \omega_{p-}^2 >> \omega^2 \tag{154}$$

This latter result is then time independent and applies to the case where one of the plasma frequencies (for $z < 0$) is much greater in frequency than all other relevant frequencies in this phenomenon. The relevant point to note in this calculation is, as before, that the dense plasma layer will not substantially change surface magnetic fields unless it is thicker than

$$\ell = \frac{c}{\omega_p} \tag{156}$$

This condition is the same one derived for early time fields.

SECTION V

COUPLING TO LOCAL GEOMETRIES

In the previous sections we discussed the coupling to infinite conducting planes of a plane wave of incident X-rays; in this section we will review a number of concepts which we developed in those sections and discuss how they may be applied in the analysis of more complex geometries. We will specifically deal with those classes of problems we expect to be amenable to analytic approaches, and those which can only be solved by numerical methods. In this section we will draw heavily on experience in satellite SGEMP and ground level close-in-coupling analysis methods.

We have noted that the analysis of the previous sections has given us a number of time and distance scales which appear in the electromagnetic problem. In the early time response which is dominated by the surface photoelectrons, the distance scales which appear are the characteristic dimension of space charge limiting at the time of the peak of the magnetic field (typically a few millimeters), and the characteristic distance into the plasma over which low frequency surface electromagnetic fields vanish. This latter distance is c/ω_p and is typically on the order of 30 centimeters. The relevant time scales are the time at which $\dot{P}$ (the time derivative of the dipole moment) peaks in a vacuum calculation of space charge limiting (typically 0.2 nsec), $\cos\theta/\omega_p$, the inverse of the frequency at which the surface magnetic fields oscillate (also typically 0.2 nsec), and $1/\omega_p$, the inverse of the frequency at which the longitudinal (electrostatic) part of the electric fields oscillates (typically 1.0 nsec). The transverse (electromagnetic) part of the electric fields oscillates at $\cos\theta/\omega_p$, the same as the magnetic fields.

For the late time fields driven by the air photocurrents on a slower time scale, there is only one relevant distance scale, c/ω_p (typically 30 cm). Time time scales are set by the inverse of the collision frequency, $1/\nu_m$ (which we assume to be long), the duration of the X-ray pulse (typically 20 nsec) and the inverse of the plasma frequency, $1/\omega_p$. The

reason for the relevance of the latter and not $\cos\theta/\omega_p$ is that the transverse part of the fields radiates away in external problems but the longitudinal part of the fields persists. This can be seen from the dispersion relations for a cold plasma (T→0) in the absence of a magnetic field, which are, for the longitudinal electric field, from reference 12,

$$\omega^2 = \omega_p^2 \qquad \vec{E} \| \vec{k} \tag{157}$$

and, for the tranverse electric field,

$$c^2k^2 = \omega^2 - \omega_p^2 \qquad \vec{E} \perp \vec{k} \tag{158}$$

For our early time case where the wave is incident on the surface with an angle θ

$$ck_x = \omega \sin\theta \tag{159}$$

and, when substituting this in equation (158).

$$c^2k_z^2 = \omega^2\cos^2\theta - \omega_p^2 \tag{160}$$

Note that for $\omega < \omega_p/\cos\theta$, the waves are trapped near the surface as k_z is imaginary. For $\omega > \omega_p/\cos\theta$ the waves radiate away at an angle θ_r where

$$\cot\theta_r = \frac{k_z}{k_x} = \sqrt{\cot^2\theta - \frac{\omega_p^2}{\omega^2}\csc^2\theta} \tag{161}$$

For $\omega >> \omega_p/\cos\theta$, $\theta_r = \theta$ and the waves radiate away at the spectral angle as in vacuum SGEMP. One should note that for certain geometries this can cause a high frequency interaction between different parts of the surface as shown in figure 12. This is one exception to the general rule that portions of the missile separated by more than c/ω_p do not interact electromagnetically. The other exception is the diffusion of low frequency magnetic fields through a resistive plasma as noted in section IV.

12. Krall, N. A. and A. W. Trivelpiece, Principles of Plasma Physics, McGraw-Hill, New York, 1973.

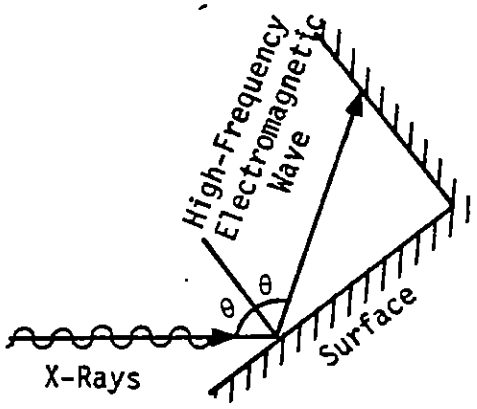

Figure 12. High Frequency Surface-Surface Interaction

We now turn our attention to the early time regime, dominated by surface photoemission and discuss methods applicable for the calculation of the electromagnetic response of complex objects. If the object dimensions are comparable to the space charge limiting dimensions, in general it is necessary to perform numerical computations to determine the electromagnetic response. These numerical calculations generally need to be multidimensional, and the electromagnetic fields and photoelectron trajectories need to be self consistently calculated. If the object radii of curvature are larger than c/ω_p, we may treat surfaces as locally flat. Between these regimes we use composite methods as we will shortly show.

In the late time regime, separations of larger than c/ω_p are essentially isolated from each other. As we no longer have the necessity of calculating the space charge limiting of surface photoemission, it should be possible to make relatively good analytic models of simple geometries.

As an example of a calculation of the response of a local geometry, we estimate the response of a short (~10 cm), thin (<1 mm) monopole antenna protruding from the surface as shown in figure 13. We assume that the radius, r_t, of the transmission line is much greater than $\sqrt{hd}$ (where h is the monopole height and d is its diameter) so that the antenna capacitance is not strongly dominated by the portion about its base.

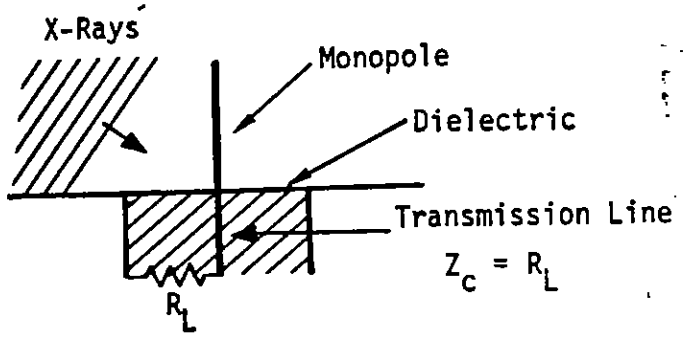

Figure 13. X-Ray Excited Thin Monopole Antenna

We will consider the following physical effects on this antenna:

1) Normal electrostatic field caused by photoemission from the surface.
2) Normal component of the transverse electric field caused by photoemission from the surface.
3) Photoemission from the monopole itself.
4) Modification of the antenna impedance by the surrounding plasma.

We have chosen this particular geometry as we can use an analysis method similar to the close-in-coupling analysis of reference 13. As this dipole is short compared to the wavelengths involved, we can make the electrostatic approximation for the electric fields involved, and use the equivalent circuit shown in figure 14, where C is the (frequency dependent) capacitance of the antenna in the plasma, as we will discuss shortly. V_i is the open circuit voltage caused by the electric field drivers, I_e is the current emitted from the monopole itself and R_L is the load resistor, equal to the characteristic impedance of the feed geometry.

13. Longmire, C. L., "Direct Interaction Effects in EMP," AFWL Interaction Note 69, Air Force Weapons Laboratory, Kirtland AFB, NM, 1973.

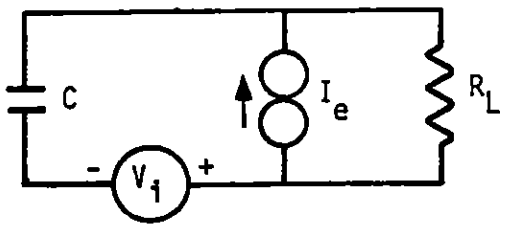

Figure 14. Equivalent Circuit of X-Ray Excited Monopole

We first consider the electric field driving terms to determine the open circuit driving voltage V_i. As mentioned above, there are two contributions to this, the electrostatic voltage across the space charge limited layer of photoelectrons emitted from the surface, and the voltage caused by the electric field of the radiated wave. As the effective height of our antenna is h/2, we can write

$$V_i = V_{pe} + \frac{1}{2} E_{tz} h \tag{162}$$

The first term, in practical cases where the emitted photoelectron density greatly exceeds the ambient plasma density, is little changed from its vacuum value, and if P(t) is the vacuum dipole moment time history,

$$V_{pe}(t) = \frac{P(t)}{\epsilon_o} \tag{163}$$

E_{tz} can be determined from the surface magnetic field which we calculate in section 3 and

$$\frac{1}{c} \frac{\partial}{\partial t} E_{tz} = - \frac{\partial}{\partial x} B_y \tag{164}$$

but

$$\frac{\partial}{\partial x} = \frac{\sin\theta}{c} \frac{\partial}{\partial t} \tag{165}$$

so

$$E_{tz} = -\sin\theta\, B_y \tag{166}$$

As the monopole radius is much smaller than space charge limiting dimensions, I_e is the total photocurrent emitted from the monopole and has the shape of the incident X-ray pulse.

We now turn to the task of estimating the antenna capacitance. In vacuum the capacitance would be approximately

$$C_o = \frac{h}{2\ell n(h/a)-2} \tag{167}$$

In the plasma we must add the electron current to the displacement current,

$$I = C\dot{V} = \int da \left(\frac{1}{c} \frac{\partial E}{\partial t} + \frac{4\pi}{c} J_e \right) \tag{168}$$

where

$$J_e = -Nev = \frac{Ne^2}{m} \int dt\, E \tag{169}$$

or in the frequency domain

$$C(\omega) = \left(1 - \frac{\omega_p^2}{\omega^2} \right) C_o \tag{170}$$

The solution for the load voltage is easily seen to be (in the frequency domain)

$$V_L(\omega) = \frac{i\omega RC(\omega) V_i(\omega)}{-i\omega RC(\omega) + 1} + \frac{R\, I_e(\omega)}{-i\omega RC(\omega) + 1} \tag{171}$$

We will determine the time history of the response to separate delta function voltages and currents

$$V_i(\omega) = \frac{1}{2\pi} \tag{172}$$

$$I_e(\omega) = \frac{1}{2\pi} \tag{173}$$

The response to other driving time histories can be obtained by a convolution. For the response to a delta function voltage we obtain

$$V_L(t) = \frac{1}{2\pi}\int_{-\infty}^{\infty} \frac{iRC_o(\omega^2 - \omega_p^2)}{-iRC_o(\omega^2 - \omega_p^2) + \omega}\, e^{-i\omega t}\, d\omega \qquad (174)$$

This integral may be solved by contour integration as before. The denominator has roots at

$$\omega_{\pm} = \pm \frac{\sqrt{4\omega_p^2 R^2 C_o^2 - 1}}{2RC_o} - \frac{i}{2RC_o} \qquad (175)$$

with three possibilities for their location in the complex plane. For $2\omega_p RC_o > 1$ we have conjugate poles (see figure 15) whereas for $2\omega_p RC_o < 1$ we have the roots on the imaginary ω axis as shown in figure 16. Finally for $2\omega_p RC_o = 1$ we have a double pole on the imaginary axis at $\omega = -i/2RC_o$. For simplicity we work with the first two possibilities.

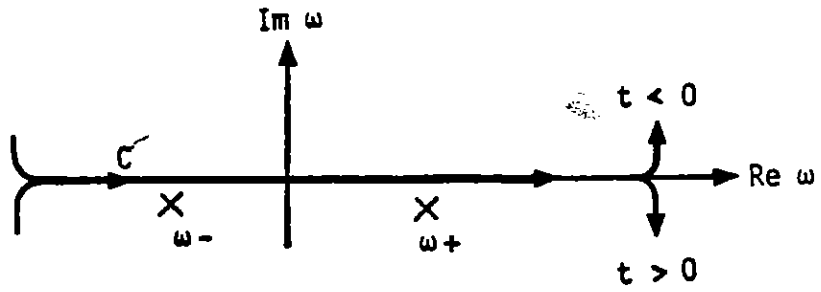

Figure 15. Pole Locations and Integration Contour for $2\omega_p RC_o > 1$

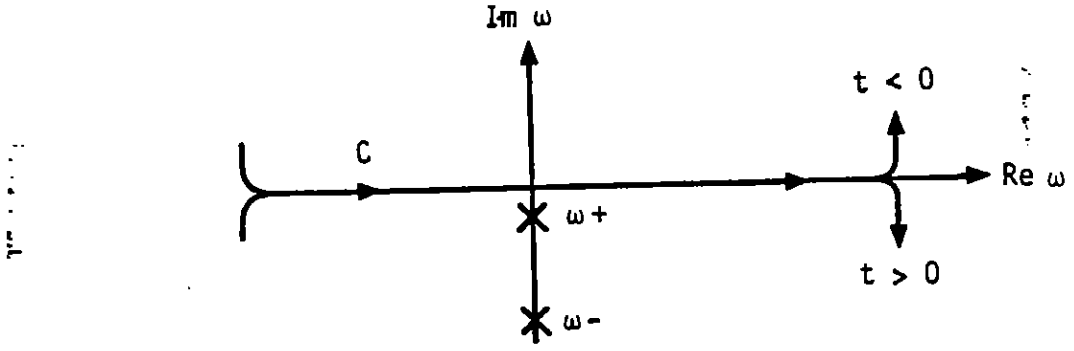

Figure 16. Pole Locations and Integration Contour for $2\omega_p RC_o < 1$

For $t < 0$ we can close the contour C with an infinite semicircle in the upper half plane, and obtain $V_L = 0$. For $t > 0$ we close the contour with an infinite semicircle in the lower half plane and obtain

$$V_L(t) = G_V(t) = +i\left(\frac{\omega_+^2 - \omega_p^2}{\omega_+ - \omega_-}\right)e^{-i\omega_+ t} - i\left(\frac{\omega_-^2 - \omega_p^2}{\omega_+ - \omega_-}\right)e^{-i\omega_- t} \qquad (176)$$

This expression is obviously real for $2\omega_p RC_o < 1$, as $\omega_+ - \omega_-$ is imaginary. For $2\omega_p RC_o > 1$ it is real as $\omega_+ - \omega_-$ is real, and the second term is the complex conjugate of the first. Similarly for a delta function current source one obtains for $t > 0$

$$V_L(t) = G_I(t) = \frac{1}{C_o}\left\{\left(\frac{\omega_+}{\omega_+ - \omega_-}\right)e^{-i\omega_+ t} - \left(\frac{\omega_-}{\omega_+ - \omega_-}\right)e^{-i\omega_- t}\right\} \qquad (177)$$

This expression is always real for the same reasons as above. For arbitrary time histories of V_i and I_e

$$V_L(t) = \int_{-\infty}^{t} dt' \left[G_V(t-t')\, V_i(t') + G_I(t-t')\, I_e(t')\right] \qquad (178)$$

For the dimensions given, with a termination of 100 ohms,

$$R\,C_o \sim 10^{-10}\ \text{sec} \tag{179}$$

so that

$$2\omega_p\,R\,C_o = .2 \tag{180}$$

A typical behavior of V_{pe} which dominates over 1/2 $E_{tz}h$ is shown in figure 17. A typical I_e is shown in figure 18.

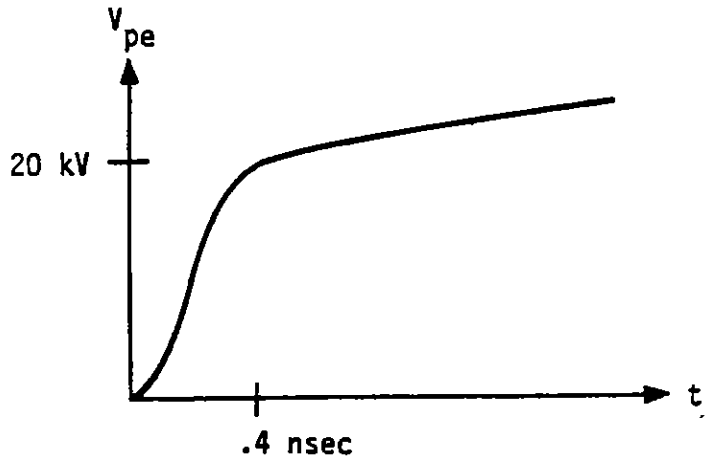

Figure 17. Typical V_{pe} From One Dimensional Particle Calculations

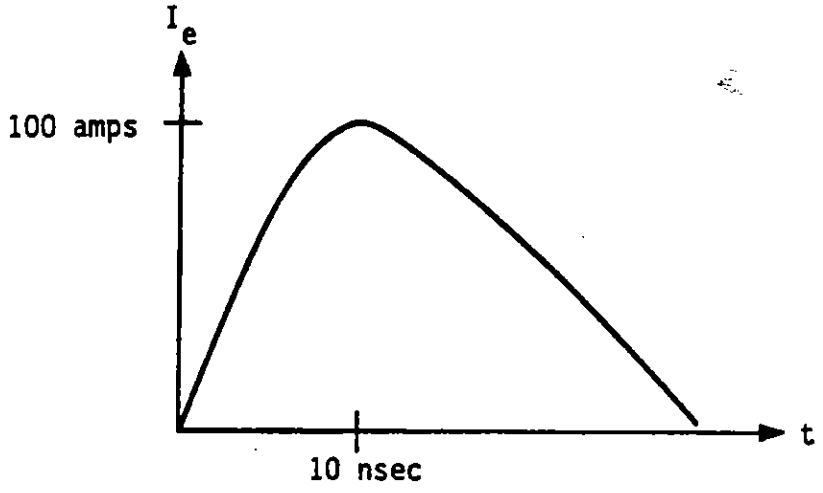

Figure 18. Typical I_e Resulting From Emission Off of Aluminum Monopole

With these typical values, we find the voltage resulting across the load which is sketched in figure 19.

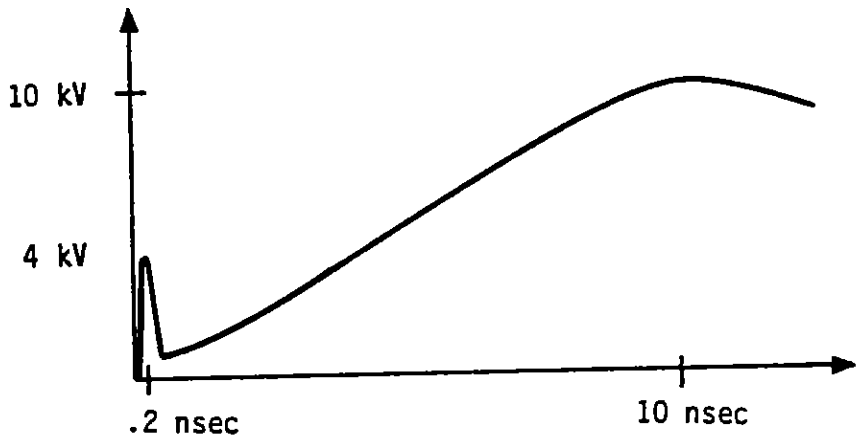

Figure 19. Load Voltage Resulting From X-ray Illumination of a Monopole Antenna

The plasma oscillations are not seen for this example because $\omega_p \ll \frac{1}{RC}$ and the antenna responds much as it would without the plasma. For a load impedance on the order of 5 kilohms we would see oscillations in the response.

During the late time period dominated by air photocurrents, the antenna will respond primarily to E_z with

$$V_i = \frac{h}{2} E_z \qquad 181)$$

Features of this calculation worthy of note are the transfer of energy between the plasma electrostatic oscillations and the load, and the consequent damping of these oscillations as energy is removed from them.

SECTION VI

SUMMARY

In this report, we have presented a number of calculations relevant to the generation of electromagnetic fields when weapon X-rays impinge on missiles in flight in the altitude regime where the secondary electrons' motion is not collision dominated and electrostatic and electromagnetic plasma oscillations are seen. We have noted that the problem separates naturally into two time regimes; the first one being dominated by surface photoemission and the second one being dominated by air photocurrents. We have calculated the response of a flat surface in the two time regimes and we have made a simple model of a monopole antenna exposed to X-rays.

REFERENCES

1. Longmire, C. L. and H. J. Longley, Improvements in the Treatment of Compton Current and Air Conductivity in EMP Problems, DNA 3192T, Defense Nuclear Agency, September 1973.

2. Morse, P. M. and H. Feshbach, Methods of Theoretical Physics, McGraw-Hill, 1953.

3. Dellin, T. A. and C. J. MacCallum, Handbook of Photocompton Current Data, SCL-PR-720056, Sandia Laboratories, 1972.

4. Schaefer, R., "A Simple Model for Soft X-ray Photoemission," Jo. App. Phys., 44, 1973.

5. Heitler, W., The Quantum Theory of Radiation, Oxford University Press, London, 1954.

6. Evans, R. D., The Atomic Nucleus, McGraw-Hill, 1955.

7. Carron, N. J. and C. L. Longmire, "Electromagnetic Pulse Produced by Obliquely Incident X Rays," IEEE Trans. Nuc. Sci., NS-23, December, 1976, pp. 1897-1902.

8. Longmire, C. L. and N. J. Carron, Scaling of the Time Dependent SGEMP Boundary Layer, DNA 3975T, Defense Nuclear Agency, April 1976.

9. Carron, N. J., Dynamical Solution of the SGEMP Electron Boundary Layer for Linearly Rising and Constant X-ray Time Histories, DNA 4142T, Defense Nuclear Agency, December 1976.

10. Abramowitz, M. and I. A. Stegun, Handbook of Mathematical Functions, U.S. Government Printing Office, 1970.

11. Higgins, D. F., C. L. Longmire and A. A. O'Dell, A Method for Estimating the X-ray Produced Electromagnetic Pulse Observed in the Source Region of a High Altitude Burst, DNA 3218T, Defense Nuclear Agency, November 1973.

12. Krall, N. A. and A. W. Trivelpiece, Principles of Plasma Physics, McGraw-Hill, New York, 1973.

13. Longmire, C. L., "Direct Interaction Effects In EMP," AFWL Interaction Note 69, Air Force Weapons Laboratory, Kirtland AFB, NM, 1973.